Department of Small Animals and Horses

University of Veterinary Medicine Vienna

Clinic of equine Hospital

Head: Univ.-Prof. Dr. med. vet. Florien Jenner, Dipl. ACVS/ECVS

Development of a 3D tendon-on-a-chip model: a pilot study.

Master Thesis

for the degree of

Master of Science (MSc.)

University of Veterinary Medicine Vienna

Submitted by

Viktoria Zachl, BSc.

Vienna, May 2021

Thesis Supervisors:

Univ.-Prof. Dr. med. vet. Florien Jenner, Dipl. ACVS/ECVS

AND

Dr. med. vet. Iris Ribitsch, PhD, Priv.-Doz.

University of Veterinary Medicine Vienna

Department of Small Animals and Horses

Clinic of equine Hospital

AND

Dr. Mario Rothbauer, MSc

Medical University of Vienna
Department of Orthopedics and Trauma Surgery

Karl Chiari Lab for Orthopaedic Biology

Reviewer: Assoc. Prof. Dr. Thomas Kolbe

University of Veterinary Medicine Vienna

Institute of In-vivo and In-vitro Models

Biomodels Austria

Table of Contents

1. Introduction

Tendons are essential for locomotion. They transmit biomechanical forces between muscles and bones[1–5]. Unfortunately, they are frequently injured due to trauma or overuse. Tendon injuries affect approximately 25 % of the adult population and even more athletes (30 – 50 % of sport injuries affect tendons)[1,2]. The same is observed in horses. Tendons are frequently injured in racehorses (with an incidence of up to 40 %), show jumpers and other sports horses, where an injury of the superficial digital flexor tendon (SDFT) often results in an early end to the career[6]. Horses thus represent a good model for naturally occurring tendon disease and have long been used to study tendon physiology and pathologies. The comparable size and the functional equivalence of the human Achilles tendon and the equine SDFT provide a better translatability and emphasize the superiority of the equine model over other animal models such as rats and rabbits[7].

Lesions of the tendon often lead to pain, limited mobility and in case of athletes or performance horses to the end of the career. To restore the patient's well-being, most currently applied treatment approaches are focused on (temporary) pain relief, but often fail to restore the complete functional capacity of the tissue[1,4]. The therapy regimen follows the principle of rest, cooling and support[8]. Therefore, most commonly used treatments are non-surgical, such as cryotherapy, controlled exercise and the administration of pharmaceuticals[8]. None of the approaches is capable of restoring the functionality of the tissue. Rather, scar tissue is formed, which is functionally not as resilient and makes the tissue prone to further injury[4,9–11]. To find new treatment approaches that efficiently induce adequate tissue repair and are capable of restoring all biomechanical properties, reliable disease models to further explore the pathophysiology of tendon disease have to be developed.

Currently, millions of animals are used in experiments, largely mice, rats and hamsters. Large animals such as the horse, are also used, although to a lesser extent[12]. The use of animals in experiments is highly controlled to ensure animal welfare, it needs preceding authorization and approval by an ethics committee[12] and it is expensive[13]. Furthermore, animal experiments in science are not fully accepted by society and ethical issues are frequently debated[12], putting pressure on the development of alternatives to reduce the number of animals used experimentally. Not all of the data obtained by animal *in vivo* experiments is clinically translatable to the human and traditional animal testing approaches are ethically questionable.

Hence, the establishment of in vitro alternatives is of the utmost importance[12,14]. Any *in vitro* alternative should meet the needs of translatability, contribute to 3R (replace, reduce, refine) efforts and offer significant advantages over animal testing[13].

A suitable approach to reduce the need for animal experiments, could be the use of the so-called microfluidic organ-on-a-chip technology. The biochips allow three-dimensional cultivation of various cell types for the investigation of physiological processes as well as disease pathophysiologies and drug effects. It is possible to use patient-derived cells in organs-on-a-chip, enabling new ways of modeling disease in a patient-specific manner[15], consistent with the concept of precision medicine[16]. Further, the microfluidic technology can be used to exert tissue-specific stimuli. Physiologic cues such as biomechanical stretching can be implemented to accurately mimic the cellular microenvironment and mechanical *in situ* conditions[17].

1.1 Tendon anatomy and pathology

Tendons belong to the family of soft tissues as veins, muscles and ligaments[18]. They are highly complex, heterogenous structures of the musculoskeletal system and are part of the dense connective tissues. Appearing as whitish bands or cords, they are linked to a muscle on one side (myotendinous junction) and to a bone on the other (enthesis), forming a dynamically adapting connection which responds to environmental stimuli[3,5,19]. Acting as mechanical bridges, tendons transfer forces generated by muscular contraction in a passive manner[5,20–22].

Around 70% of the tendon tissue is composed of water. The other 30% are mainly type Ⅰ collagens[3–5,8,20], some proteoglycans, elastin and other small molecules[3,5,19,21]. The high amount of collagen makes the tendon resistant to tension and the proteoglycans provide viscoelasticity[21]. In order to form a tendon, tropocollagen molecules cross-link and progressively fuse (see fig. 1a) to form microfibrils and fibrils[3,5,21,23–25]. Fibrillogenesis is regulated by proteoglycans, such as aggrecan, found in the ECM[26]. A single fibril can have a diameter between 10nm and 500nm[5,18], depending on the species, the age and the location in the body[18]. Many fibrils running in parallel (fig. 1b and 1c) form collagen fibers, which in turn form bundles, the so called *fascicles*[3,5,8,25], that are sperated by the endotenon[24], and held together by the epitenon[1,5,21,27]. The endotenon and epitenon contain nerves, blood vessels, growth factors and roundish cells[8]. Further, they allow gliding motion of the fascicles[1,3,21],

enabling them to stretch. Fascicles moreover display wavy patterns, the so called *crimp*, that plays an important role in tendon elasticity[5,8,19,21].

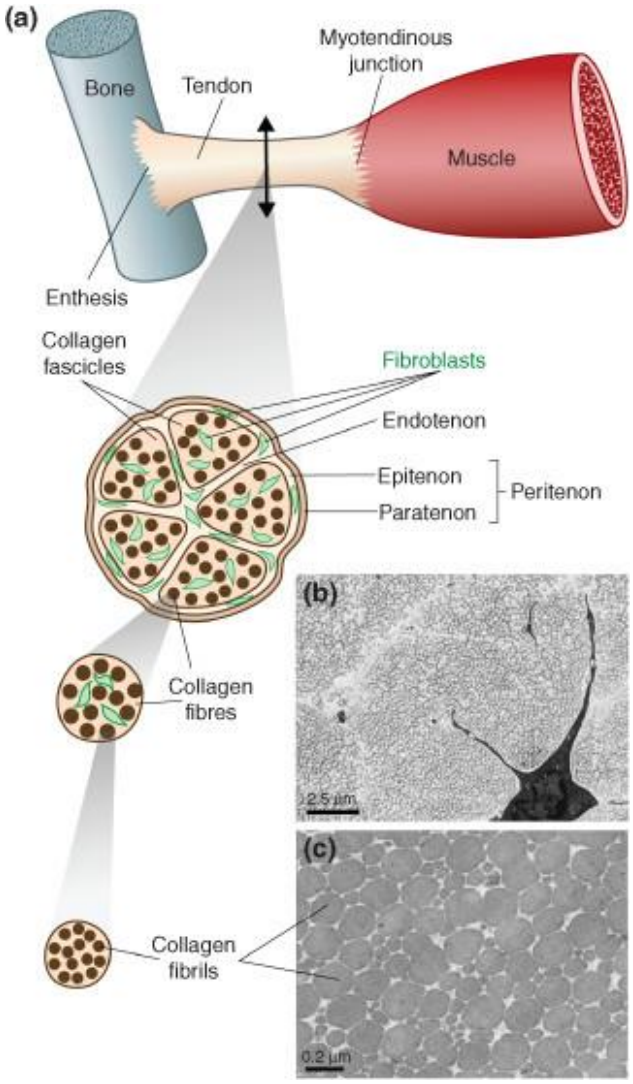

***Figure 1: Tendon structure**. (a) Tendons attach to muscle (myotendinous junction) and bone (enthesis) and are built of collagen fascicles separated by the endotenon. Fascicles in turn are made of collagen fibers which again are composed of collagen fibrils. The tendon is further wrapped by the tendon sheaths called peritenon, which comprises paratenon and epitenon. (b and c) electron microscopy of collagen fibers and fibrils (transverse section of mouse Achilles tendon)*
Source: Gaut and Duprez, 2016

In immature tendons high levels of cartilage oligomeric matrix protein (COMP) can be found[8] and it has been reported that too little load results in diminished COMP levels[20]. COMP helps to effectively organize collagen fibrils into the complex structure that makes a tendon and therefore, COMP is crucial during tendon development and growth[8]. In horses, its abundance in the tendon peaks after approximately two years of age and diminishes afterwards[20]. The mature tendon tissue, however, is not the same in all individuals as the differentiation process is influenced by mechanical and environmental stimuli[8].

In general, mature tendon tissue in relation to other tissues shows low cellularity with two major subtypes of cells: tenocytes and tenoblasts[5,20]. Additionally, chondrocytes and endothelial cells can be found in areas of compression[5,20]. Tenocytes, fibroblasts of elongated shape[5,22], are crucial effectors when it comes to formation and maintenance of tendon tissue[20]. They synthesize, maintain and degrade the extracellular matrix (ECM)[7] and act in response to a variety of stimuli, like exercise or trauma, and in turn remodel their microenvironment to meet the environmental requirements[1]. Their products comprise not only collagens, but also proteoglycans and gylcoproteins as well as degradative enzymes like matrix metalloproteinases (MMPs) and their regulators[4,7]. The ECM is a key player for tendon health with any deviation in composition directly influencing the tissue[4,5].

Another interesting feature of tenocytes is their single primary cilium. This cilium functions as a sensory organ and is connected to the longitudinal axis of the tendon. The cilium is considered a key player for mechanotransduction that is deflected when the tendon is loaded or in response to fluid flow. Mechanical loading leads to upregulation of n-cadherin and vinculin and an enhanced assembly of actin fibers into stress fibers, to keep optimal cell-to-cell contact[7].

Tenoblasts, fibroblasts of more oval shape, play important roles when it comes to healing and tissue repair[22]. They represent the majority of tendon fibroblasts (90 - 95 %)[1,22], are capable of depositing collagen fibers and may transform into tenocytes at the end of a tissue repair phase[22]. Another cell type resident in tendon tissue are tendon stem/progenitor cells (TSPCs). TSPCs display self-renewal capacities and have been shown to be multipotent, they are considered to be stem cells capable of re-establishing tendon-like tissues[21,23].

In the equine tendon, tenocytes are divided into three types based on their appearance (see fig. 2). Type one is charcterized by a spindle-shaped nucleus, type two by a cigar-shaped neucleus and type 3 displays a chondroid appearance[7]. The human equation of type one and

two tenoytes are tenocytes and tenoblasts[5], while type three cells, which are found in fibrocartilaginous areas of the tendon, resist compressive and tensile forces[7].

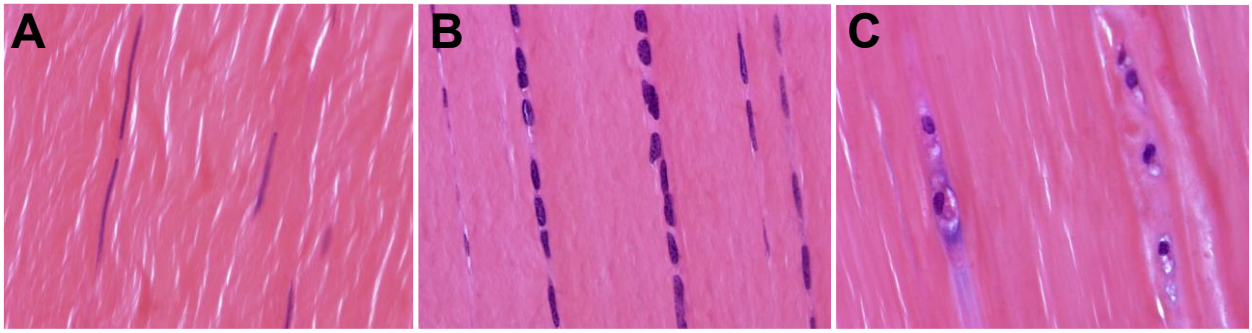

***Figure 2: Morphological types of equine tenocytes**. **(A)** type 1 cells with long and spindle-shaped nuclei **(B)** type 2 cells with cigar-shaped nuclei and **(C)** type 3 cells with chondrocyte-like appearance*
Source: Patterson-Kane et al., 2012

The tendon itself is wrapped by the *epitenon*, which is continous with the endotenon and provides blood and lymphatic vessels as well as nerve supply[5,8,27]. The epitenon sheet is for some tendons coated by another layer, the so called paratenon, or enclosed within a tendon sheath. The paratenon is a highly elastic tissue and is believed to play an important role in tendon repair[5,8]. It is mainly buit of collagen (type I and type II) and elastic fibrils[5]. The tendon sheath is usually found wherever tendons change directions over a joint and usually a fibrocartilaginous pad coveres the bony protrusions[8]. This combination enables the tendon to glide over the bone with the least possible resistance[5,8].

1.2 Tendinopathy

The generic term "*tendinopathy*", replacing the former used "*tendinitis*", comprises all tendon and/or paratenon injuries without rupture. To specify the type of lesion, other terms have been defined: *Paratendonitis* or *peritendinitis* if the paratenon is involved; *tendinitis* in case inflammation is involved[9,28]; *tendinosis* is a chronic pathology caused by the accumulation of small tears, resulting in degeneration[9,21,28]; *tenosynovitis* refers to an inflammation of the tendon sheath[9,28].

Tendinopathies are characterized by impaired biomechanical properties of the respective tissue, swelling/thickening, pain and reduced capacity to store energy[3,9,28]. Frequently,

tendinopathies are long-term impairments as healing is slowed due to the low cellularity and humble metabolic activity characteristics of tendon tissue[1,2,21]. The susceptibility of tendons to injury is rather high and underlying factors are separated into two groups: extrinsic and intrinsic factors. Extrinsic factors comprise sports and physical (over-) loading, as well as environmental conditions such as temperature, footwear and surface/ground nature. Examples for intrinsic factors are age, adipositas, gender, anatomy and disease[2,3,9,21,27].

Not included in the term tendinopathy are tendon abnormalities that originate from genetic predisposition and other primary diseases. Genetic disorders that affect players of the type I collagen fibrillogenesis result in aberrant tendon tissue structure and function and entail defects in all connective tissues[24].

In tendinopathic patients overall tendon structure differs from those of healthy individuals[9]. Tendons are not only thickend but frequently display abnormal structural organisation and cellularity[9]. Disorganization of collagen fibers brings about loss of function and elasticity in chronically affected tendons, and an increase of blood vessels and sensory nerves can be observed[9]. Further, in degenerative regions of the tendon tissue, hypocellularity can be found as cells undergo augmented cell death. In contrast, in reactive regions cell numbers increase[9]. Frequently increased are vascular cells and leukocytes, like macrophages and mast cells[9,21]. Inflammation appears to be critical for disease onset and progression[29]. Still, inflammation arises only to a limited extent and mainly due to the release of substance P and prostaglandin E (PGE_2). The inflammatory mediator PGE_2 stimulates dagradation enzymes and limits tenocytic collagen synthesis[9]. Moreover, several different cytokines seem to play a vital role in tendon disease[29]. The level of TGF-β, which is found to drive tenocytic differentiation and morphogenesis, rises in case the tendon is hurt[11]. Clinical samples of tendinopathic tissues revealed that in humans only IL-6 is elevated after injury, while for animals the concentrations of IL-1β, IL-6 and TNF-α rose. After a period of exercise, human tendons display elevated levels of IL-6 as well, in animals the IL-1β expression is elevated in the early phase after training. The frequently additionally investigated cytokine IL-10 remained unchanged in all cases. Animal species included in the studies were horses, dogs, rats and rabbits and examined tendinopathies mainly affected the achilles tendon, the patella tendon, the rotator cuff and the SDFT[29].

Tendinopathic tissue viewed under the light microscope displays four general differences compared to native tendon. Collagen is disrupted, the proportion of ground substance is elevated, the number of tenocytes is increased and neovascularization may be observed[30].

A possible contributor to the onset of tendinopathy may be the concept of de-adaptation. This concept describes the dynamic process of the tendon adapting to the environmental needs. Reduced load therefore induces structural re-organization and thereby loss of biomechanical properties. In case there is a sudden increase in loading of the altered tendon tissue, the tendon can not withstand and is more prone to injury[9].

1.3 The horse as a model for tendinopathies

Equine and human tendons can be divided into two groups: weight-bearing tendons and positional tendons[20]. Weight-bearing or high-strain energy storing tendons, as the equine SDFT for example, primarily function in withstanding the weight of the horse/human and show higher elasticity[3,20]. The second group, the positional tendons, are stiffer and maintain the alignment of the limb or digit. Examples would be the equine digital extensor tendons or the human finger tendons[20].

The most frequent tendon injuries of the horse affect the superficial digital flexor tendon (SDFT, fig. 3) and the deep digital flexor tendon (DDFT, fig. 3)[31]. The equine SDFT is the functional equivalent of the human Achilles tendon (AT)[7], which is the strongest human tendon[26], and has been a key player in understanding the biology and pathology of exercise-induced tendinopathies.

In contrast to many other animal models for tendon disease, such as the rat or rabbit, the equine digital tendons share the highly specialized nature of certain human tendons. The tendons are of comparable size and efficiently enable high-speed locomotion by saving energy and reducing muscular strain[7]. To store energy, both the SDFT of the horse and the human AT undergo high strains[3,7]. These similarities make the horse a better choice in order to achieve clinically relevant results than most other available models[3,7].

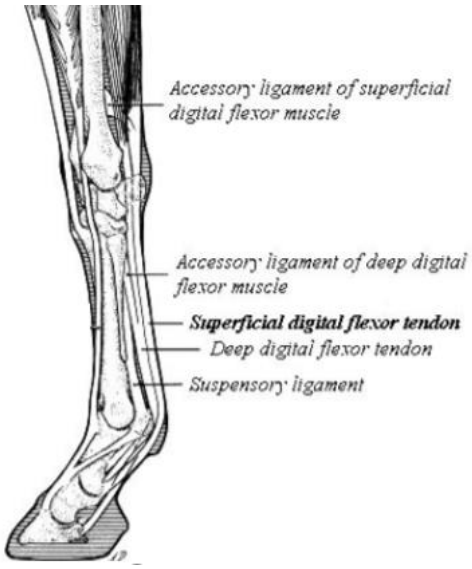

***Figure 3: The equine forelimb**. Location of the SDFT (superficial digital flexor tendon) and DDFT (deep digital flexor tendon)*
Source: Thorpe et al., 2017 (edited)

The most researched and therefore best understood tendon is the SDFT of the horse, which is frequently affected in various performance horses. In racehorses for example, the prevalence of SDFT injuries lies between 11 % and 30 % and is likely to increase with the horses' age. Moreover, re-injury rates are high[7]. The same is observed for the human Achilles tendon, around 70 % of all AT injuries happen during sports activities. For elite runners an incidence of 29 % has been reported, which is comparable to the prevalence of equine SDFT injuries in racehorses[7]. Again, the risk of AT injury increases with age[3,7].

During high-speed locomotion, when the tendon is repeatedly loaded, some strain energy is lost in form of heat that cannot be dispersed by the vasculature[7,20]. This phenomenon is called hysteresis and brings about unhealthy temperatures of 43 °C to 45 °C at the core of the SDFT of a galloping horse. Mathematic models aiming to predict hyperthermia of the AT while treadmill running, estimated similar temperatures. After 30 minutes the core of the AT would heat up to 41 °C in most individuals, with the potential to reach up to 44 °C. Temperatures of this level are assumed to be lethal or in the best case extremely stressful for the tissue fibroblasts[7].

1.4 Biomechanical properties of tendon

As mentioned before, tendons are passive transductors of muscular force, contributing to joint movement[20]. The properties of tendon are highly dependent on the percentage of fibers as well as their characteristics, orientation and grouping[18]. Their biomechanical properties can be described using so called “stress-strain curves”, which plot the applied force per unit area (the stress) against the percentage of elongation (the strain). The stress-strain curve thereafter provides values for the elastic modulus of the respective tendon[20].

A typical schematic course of a tendon stress-strain curve (see fig. 4) starts with the toe region. This first region is characterized by non-linear tendon strain of less than 2 % and represents the straightening of the crimp. It is followed by a linear region with tendon stretching of up to 4 %[18]. Deformation occurs as the collagen fibers lose their crimp pattern. This area determines the modulus of tendon elasticity and the elastic stiffness[20]. The slope of the linear deformation is also known as the “Young modulus” of the tendon.

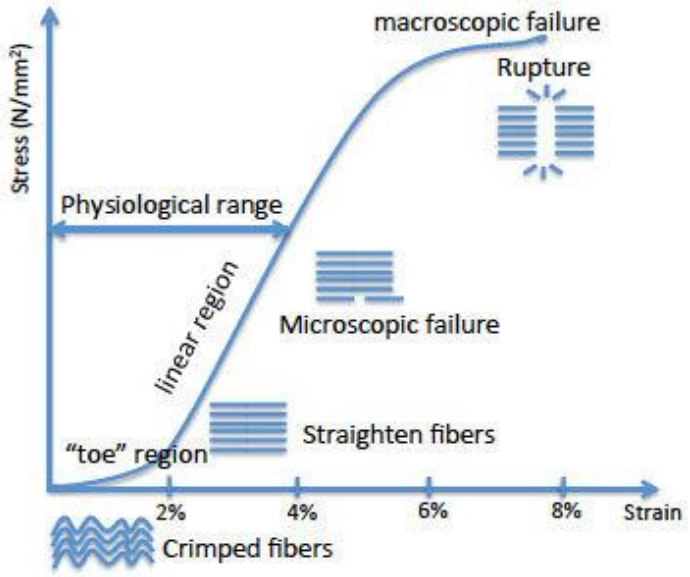

***Figure 4: Typical stress-strain curve**. The toe region (with crimped fibers) is followed by a linear region (straightened fibers). Beyond 4 % strain, the physiological range is exceeded, and microscopic failure occurs. Further increased strain results in macroscopic failure and finally in tendon rupture*
Source: Doblaré and Merodio, 2015

Exceeding 4 % of stretching is associated with microscopic tearing of the tendon fibers and goes beyond the physiological range of the tissue[18]. These strains possibly cause rupture of the covalent cross-links and slippage of collagen fibrils, resulting in irreversible lengthening of the tendon[20]. Strains of 8 to 10 % provoke macroscopic failure and further stretching may bring about tendon rupture[18].

For the SDFT of a galloping horse strains of up to 16 % have been reported. Such strain values distinctly exceed the physiological range of the stress-strain curve implicating that the tendon operates closely to failure[3]. In contrast, for the equine common digital extensor tendon (CDET), a positional tendon, the highest strain measured is 3 %[3].

1.5 Types of injuries

Tendons are typically injured either by percutaneous trauma (extrinsic) or by overstrain (intrinsic), which may result from sudden structural overload or from preceding molecular degeneration[8,20]. High tension paired with tissue compression results in elevated friction[9]. In clinical injuries, a degenerative phenotype is caused by a persistent molecular inflammation that progressively weakens the tissue and the structural integrity of the already impaired tendon being overwhelmed by excessive loading[8].

In strain-induced injuries, tendon loads exceed the tendon's strain limit, which results in disruption of the tendon matrix. The severity may vary: fibrillar slippage (resulting from the break-down of fibril cross-linking), fibrillar rupture or complete separation of tendon tissue[8,20]. In any case a repair response is mounted[8]. In order to prevent strain-induced injuries tendon peak loads have to be reduced, this can be achieved by variation of many factors. Examples for the reduction of peak loads are softer surfaces, less weight or slower movements[8].

The mechanism underlying the occurrence of tendon tears is still unclear, but too high pressures or the tendon getting physically "trapped" are conceivable explanations. Many tendon tears have been observed ensuing a tenosynovitis. This suggests that synovial hypertrophy increases the risk of tendon tears[8].

The last group, percutaneous tendon injuries, result from trauma and often occur together with contusion. Furthermore, tendon lacerations may happen if something cuts through the skin and tendon, thereby partially or completely severing the tendon[8].

1.6 Healing process

The healing process of tendon tissue is divided into three major, frequently overlapping, phases: inflammatory phase, reparative/proliferative phase and remodeling phase. However, the full functional capacity of the tissue cannot be restored[1,4,11,21,24,25,27]. Rather, disorganized scar tissue, with higher amounts of collagen type III[4,8], is formed instead. The remodeled tissue is predisposing the tendon to recurrent injury, as it is less elastic and exposes the adjacent tissue to higher strains[1,2,9,10,20].

In the first phase, a hematoma is formed, and pro-inflammatory cytokines recruit inflammatory cells, such as neutrophils, macrophages, mast cells and platelets[4,8,20,21,25,27]. These inflammatory cells in turn attract tendon cells to the site of injury[2]. Further, vascularization is promoted, fibrous tissue forms in the damaged region and collagen type III is upregulated[4,8,21,27,32]. As a next step, during the proliferative phase, extracellular matrix (ECM) compounds are synthesized, cellularity is increased, and water is attracted. The onset of the remodeling phase, which is subdivided into two stages, is approximately two months post injury and can last for up to two years[21]. Duration and course are dependent on the individual constitution and the severity of the injury. During the first stage, the production of ECM compounds and cell numbers are reduced and there is a switch back to type I collagens[4,8,21,27]. With increasing re-organisation, some tensile strenght and biomechanical properties are re-obtained. About ten weeks after the onset of this consolidation stage, the final phase of tendon healing begins: the maturation phase. As the term implies, during this phase mature tendon scar tissue is established and the cross-linking of collagen fibrils is promoted[21].

1.7 Diagnostics and tendon biomarkers

The diagnosis of tendinopathies makes use of many different techniques, such as tendovaginoscopy, tenoscopy, radiography, ultrasonography, scintigraphy, magnetic resonance imaging (MRI), and computed tomography[31]. Further, molecular biomarkers are valuable indicators for tendon disorders[24]. Unfortunately, the major structural and functional component of tendons, type I collagen, is abundant in many other tissues as well[24,33]. Therefore, monitoring the type I collagen expression is not sufficient to study tendon pathophysiologies[11,24]. For the early tendon development, Scleraxis (Scx) has been identified as good marker in chicken, mice and zebrafish. Later in development, *Scx* expression is

diminished and restricted to the epitenon[24]. Scleraxis is a transcription factor which positively regulates *Col1a1* expression but has been shown not to be the master regulator of tendon formation, which remains unknown[11,24]. Nevertheless, complete loss of Scleraxis results in inability to form healthy tendons[11]. Other developmental markers, that are not exclusive to the tendon lineage, are Mohawk (Mkx) and zinc finger transcription factors called early growth response one (*Egr1*) and early growth response two (*Egr2*)[11,24]. Developmental markers are characteristic for the immature tendon only and are not necessarily expressed in mature tissue[11].

For differentiated Tenocytes, Tenascin-C (*TNC*), Thrombospondin-4 (*THBS4*) and Tenomodulin (*Tnmd)* are good molecular markers[11,24]. TNMD codes for a type II transmembrane glycoprotein and its loss results in altered collagen fibril structure and is associated to poor self-renewal capacities and elevated senescence of progenitor cells[24].

By analyzing transcriptome and proteome data more tendon biomarkers have been identified. Significantly enriched were otoralpin (OTOR), A-kinase protein 12 (AKAP12), perilipin-4 (PLIN4), myocilin (MYOC), caronic anhydrase 3 (CA3), decorin (DCN), tenomodulin (TNMD), keratokan (KERA), fatty-acid binding protein 5 (FABP5), apolipoprotein A1 (APOA1), CB1 cannabinoid receptor-interacting protein 1 (CNRIP1), actin aortic smooth muscle (ACTA2) and calponin-2 (CNN2)[34].

1.8 Current treatment approaches

1.8.1 Non-surgical therapies

Most tendinopathies are treated non-surgically (except for lacerations) with major attention to pain relief[1,8] and follow the principle of rest, cooling and applied[8].

Cold therapy (Cryotherapy) is especially effective during the acute inflammatory phase[8,28,32]. Its anti-inflammatory effect is based on the induction of vasoconstriction, as well as the reduced formation of inflammatory mediators and the decrease in enzymatic activity. In general, cold hydrotherapy is to be preferred over the use of ice packs, due to the decreased risk of side-effects[8].

Compression and coaptation applied during the acute phase results in a diminished inflammatory response and edema formation. If the lesion results in joint instability, an external coaptation should be included, or a splint or cast can be included[8].

Controlled exercise is a suitable strategy to promote tissue remodeling and maintain gliding function. Nevertheless, the exercise level and the tendon condition have to be closely monitored in order to prevent further injury[8].

Extracorporeal shock wave therapy (ESWT) is well established in human orthopedic treatments, although its mechanism of action is quite unclear. Furthermore, there has been evidence that ESWT leads to matrix disorganization and therefore may also pose a risk to healthy tendons[8]. Another side-effect of ESWT is intensive pain during the treatment[35].

Ultrasound, laser and magnetic fields are potential treatment options, but the underlying mechanisms are unclear. In case of ultrasound a therapeutic effect could be found experimentally, but for lasers and magnetic fields no such data is yet available[8].

Pharmacologic interventions can either be applied systemically or intralesionally. In case of systemic medication, corticosteroids and non-steroidal anti-inflammatory drugs (NSAIDs) are commonly used to treat tendon injuries[8,28,32]. Nevertheless, both have been reported to induce adverse effects/side-effects [9,31,36]. Corticosteroids impair local collagen synthesis and NSAIDs negatively impact enthesis healing and may also impair muscle repair[9,28]. Examples of drugs to be applied intra-lesionally are poly-sulfated glycosaminoglycans or hyaluronan[8,32]. To achieve the best outcome, the site of application should be directly at the center of the lesion, which can be located by ultrasonography[8].

1.8.2 Surgical interventions

Tenoscopy uses an arthroscope to access the synovial tendon sheaths and is an important tool allowing for diagnosis of lesions that other imaging techniques/devices cannot detect[37].

Bursoscopy (analogous to tenoscopy) is used for the endoscopy of intrabursal lesions[8].

Ligament desmotomies are used if the respective ligament impedes the gliding motion of the tendon and is often performed during tenoscopy as this ensures accuracy and is less traumatic. Examples are the annular ligament desmotomy or the desmotomy of the accessory ligament of the deep digital flexor tendon[8].

Surgical repair can be necessary in case of tendon lacerations, but does not always improve biomechanical function[8,25]. The tendon is sutured and then the wound is closed. Eventually, in case of massive damage an implant has to be considered[8].

1.9 Regenerative approaches

Platelet rich plasma (PRP) is injected locally and contains more than 400 immunomodulating and growth factors, like transforming growth factor β, that promote ECM synthesis and induce tissue repair[28,32,35]. As PRP is autologous, so patient-own, it is considered to be safe[38]. It is yet unknown which components of the PRP actually benefit tendon regeneration, but some positive effects have been reported[28]. Still, in order to boost positive and minimize negative effects, more research has to be conducted to reduce variability and applied dosages should not be pre-defined, but rather be individually adjusted[38]. PRP injections have been intensively studied in horses and are a popular treatment among human athletes as they are only minimally invasive and cost-effective[31].

Autologous tenocyte injection (ATI) is the application of patient-own tenocytes in human medicine to stimulate the healing process. A biopsy of a healthy tendon yields tenocytes for expansion and application to the diseased tissue[39]. The clinical application of ATI showed a reduction in pain and better functional outcomes for different tendon pathologies in the elbow, shoulder and others[40]. In another successful example for ATI, preclinical animal studies used autologous *in vitro* expanded tenocytes in the treatment of acute tendon tears and chronic degenerative tendon diseases of lateral epicondylitis. The tenocytes were harvested from the patellar tendon without any adverse effects and in both disease models ATI led to improved tendon structure and a better healing process[39].

Bone marrow aspirates (BMAs) contain certain populations of mono-nuclear cells and are usually obtained from the sternum or ileum aspiration. These mono-nuclear cells have been reported to show good prognosis for SDFT tendinopathies. Nevertheless, the clinical use is minor, due to possible unknown effects induced by the presence of cell lineages different from MSCs (leukocytes, red blood cells) and bone spicules[31].

Mesenchymal stem cells (MSCs) are promising for the use in tenodesmic therapies[31]. Sources of MSCs in the horse are bone marrow (BM-MSCs) and adipose tissue (AdMSCs)[4,31,40]. Allogeneic, so non-self but intra-species derived, as well as autologous MSCs

are used in the treatment of equine tendinopathies and both showed positive effects. Evidence for the potency of MSC treatment was offered by a study using peripheral blood-derived stem cell injection in the course of the treatment of SDFT tendinopathy, which resulted in better reduction of clinical signs for tendon injury than the use of NSAIDs, a PRP injection or a controlled rehabilitation program[31].

Tendon stem cells (TSCs) embedded in a hydrogel that mimics the composition of native tendon ECM has been shown to positively affect tendon healing after injury in rats[4].

1.10 Cell culture systems

Cell culture is an important tool for multiple research fields[41], as it enables the evaluation of basic cellular processes[42]. “Culture” means growing the cells in appropriate medium, mimicking the natural environment and thereby keeping the cells alive[41]. The culture of tenocytes allows for the physiological and pathophysiological examination of cell characteristics and further the in vitro establishment of tendon tissue. The different forms of cell culture systems represent important data sources for the investigation and manipulation of cells and allow for insights into structural and functional features, without the need for animal experiments[42,43]. Still, it has to be kept in mind that animals are used for cell extraction and the production of sera. Advantages of cell culture systems are manifold, as all environmental parameters, like temperature, pH, nutrient supply and availability as well as many others, can be tightly controlled, standardized and modulated[42].

1.10.1 Conventional cell culture

In conventional culture, adherent cells are cultured in a monolayer[42,44], mostly using polystyrene or glass[45]. There are two main types of cultures: primary cell culture of cells with limited lifespan and permanent culture of cells with infinite lifespan (immortalized/transformed cells or tumor cells)[42]. Even though three-dimensional (3D) culture systems are emerging, the majority of cells are still cultured in a two-dimensional (2D) fashion, using conventional petri-dishes for example[46]. Nevertheless, 2D cell culture is considered more and more inadequate for recent research questions, merely covering the complexity and depth[33,46]. The major limitations of the conventional cell culture lie within the

disability to properly mimic the *in vivo* tissue milieu[13,33,47]. Cell-to-organ interactions and more complex body processes can hardly be reproduced[13,33,47] and cells are often flattened, display abnormal polarization and/or dedifferentiate[33].

1.10.2 3D cell culture

The three-dimensional (3D) culture of cells enables to model a cell *in vivo*-like while being cultured *in vitro*, adding another layer of complexity[33,45,47] and increasing the translatability of *in vitro* obtained data to physiological *in vivo* tissue[13,33,48]. There are scaffold based and scaffold-free 3D culture approaches[47]. Static scaffolds are porous substrates, forming cell culture matrices that support cellular growth, organization and differentiation[44,46]. Scaffold-based techniques use hydrogels, polymeric materials, glass fibers and organoids for support[47], allowing for architectural diversity[46]. Hydrogels are networks of polymers rich of water and effectively mimic native ECMs[33,49]. They are formed as a liquid solution undergoes extensive crosslinking in order to form a solid[33].

Moreover, there are dynamic scaffolds for 3D culture, which implement vibration, strain and/or compression to establish a more active cellular environment[44]. All variants of scaffolds pose a variety of different functional advantages to the 3D cultured cells and are selected to fit the planned experiments and the cell types used[33,47]. Scaffold-free approaches, like hanging drop microplates, magnetic levitation, and spheroid microplates, do not make use of scaffolding[47].

Nevertheless, the 3D culture of cells has many drawbacks and limitations[33,50]. Organoids vary in size and shapes and long-term culture of cells in organoids is hampered as maintaining cells in consistent positions is difficult[50]. Furthermore, most culture systems still lack the multiscale architecture and tissue-tissue interfaces/interactions needed to accurately mimic *in vivo* conditions[50].

Three-dimensional culture of tenocytes with applied static force has been shown to effectively induce the expression of tendon-associated genes[11]. The use of collagen as a hydrogel is a natural choice[8,25,33] as collagen type I is a major component of the ECM in healthy tendons[8,25]. It is biocompatible and biodegradable[4,25,33] and if used as a scaffold, it

effectively mimics the tissue forming fibrils and fibers[25,33]. In contrast to conventionally maintained tenocytes, those cultured in a 3D-manner using collagen displayed strongly increased expression levels: characteristic markers were elevated 400-fold after 7 days and 70-fold after 14 days of culture[11].

1.11 Organ-on-a-chip

The “Organ-on-a-chip” (OOAC) is a biomimetic system for the culture of living cells with the aim to recreate functional tissues and organs[13,51]. It mimics the *in vivo* situation of an organ including its physiological environment and enables the regulation of multiple factors, including concentration gradients, shear forces, cell patterning, tissue-boundaries and cell-organ interactions[52]. Moreover, they enable for easy cell observation as microfluidic chips are high resolution microscopy compatible[17] and allow for the *in vitro* analysis of biochemical, genetic and metabolic activity of living cells[50].

Organs-on-a-chip have already been established for the liver, lung, kidney, intestine and the heart[13,52,53]. To reflect the organismal complexity, multi-organs-on-a-chip (“human-on-a-chip”) are being researched[52,53]. These chips aim to enable the examination of physiological interactions by the incorporation of multiple organs that are connected by microfluidic channels[52]. There are static (single device), semi-static (devices joined by fluidic networks) and flexible approaches (using flexible microchannels)[52]. As the body absorbs, distributes metabolizes and eliminates drugs across multiple organs[54], the human-on-a-chip may enable the examination of different drug formulations and drug delivery routes (oral/transdermal/aerosol) regarding their effects toxicity and the efficiency of delivery[13]. Indeed, in order to make that possible, simply linking the single OOACs by microfluidic channels is not sufficient. Rather, each organ model has to be scaled proportionally to accurately reflect the native physiology[54].

OOACs also show great potential for the use in precision medicine[16,53]. Precision medicine aims to make healthcare more efficient by tailoring individual and ultimately more effective treatments[16]. This concept would eliminate the use of ineffective or even adverse treatments by the individual prognosis of suitable drugs and treatments, thereby reducing not only healthcare costs but possibly also improving therapy course and outcome for the individual patient by the use of patient own cells[16].

1.11.1 General set-up

For the set-up of an OOAC, four key components are necessary: microfluidics, living cell tissue, stimulation or drug delivery and sensing. The microfluidics deliver the cells to their appropriate location and ensure culture fluid input as well as waste removal[52]. 3D alignments of cells usually depend on the addition of biocompatible materials such as hydrogels, scaffolds and aggregates[17]. For data generation, a sensing component is needed, which can either be an embedded sensing output component or a transparent chip-based visual function evaluation system[52].

Currently, the major technique for making microfluidics/organs-on-a-chip is called replica molding (fig. 5a)[50]. It starts with the creation of a negative copy of the desired mold[50,55]. This is done via photolithography of a silicon wafer template[15], that is covered with a photo resistant material[55], to obtain the desired patterns etched into the silicon[50]. More precisely, the silicone chip is spin-coated with a thin layer of photosensitive material, the photoresist. This thin layer is then covered with a photomask, for example a glass plate) that contains the pattern which is supposed to be copied to the chip. When exposing the silicon chip to ultraviolet (UV) light, those regions that are covered by the photomask are protected whilst the UV-exposed other regions dissolve[50]. The obtained mold can then be filled with polydimethylsiloxane (PDMS), a liquid polymer, which creates a positive copy after polymerization[55]. Therefore, the PDMS stamp displays microscale patterns that are complementary to those previously etched into the silicon chip[50]. This PDMS imprint is bonded to a glass slide, resulting in the formation of small chambers and channels[55].

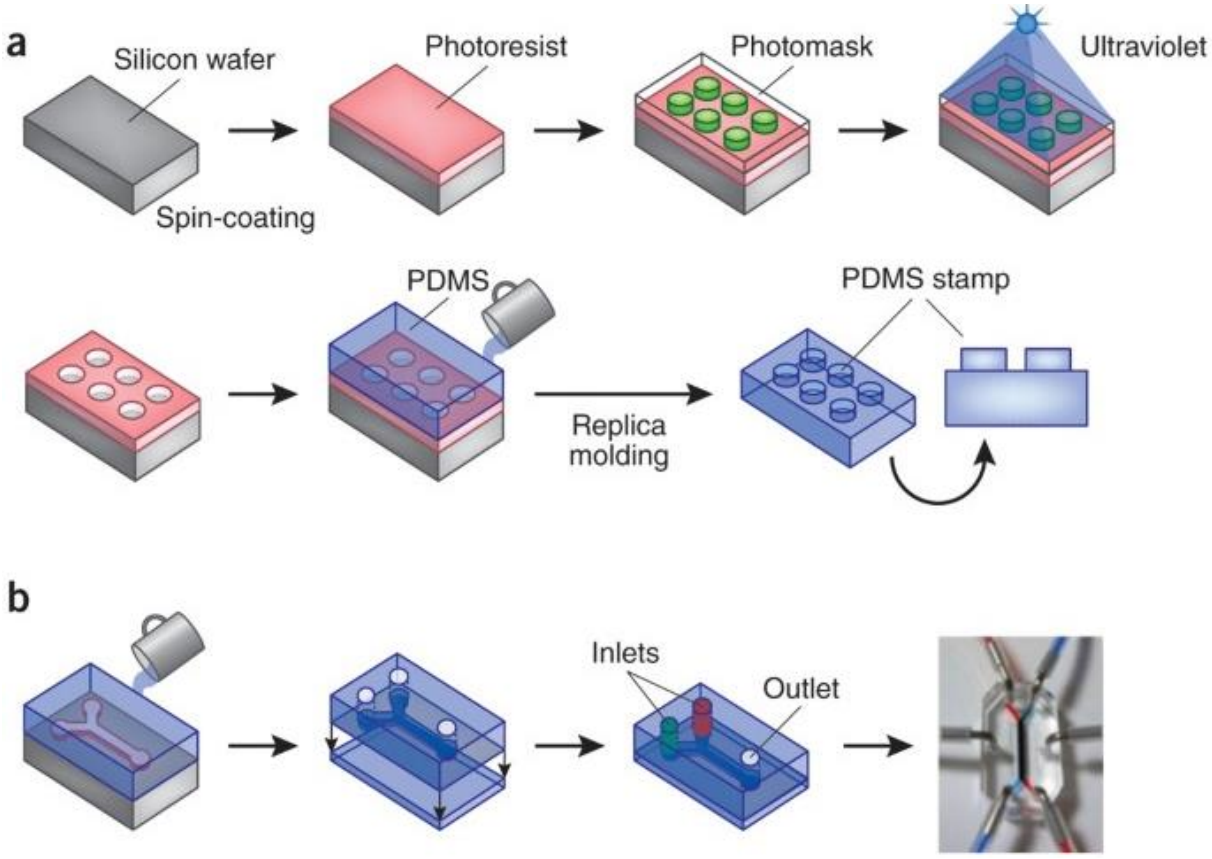

Figure 5: Fabrication techniques for microfluidic devices. (a) *A silicon wafer is spin-coated with a photoresist (photo-sensitive material) and then overlaid with a photomask. By the exposure to UV light, the photoresist that is not covered dissolves and a microscale pattern is etched to the surface of the chip. Using this mold, an elastomeric stamp is created using liquid PDMS and waiting for it to polymerize.* ***(b)*** *Single-channel devices need PDMS stamps with only two inlets, a main channel and an outlet, that are sealed to a glass slide. The picture on the right shows a two-chamber device with red and blue dye perfused trough upper and lower channels and clear channels at either side for the application of cyclic suction to rhythmically distort the flexible central membrane and with it the adherent cells.*
Source: Bhatia and Ingber, 2014

This technique, the soft lithography[56], produces structures out of elastomeric materials. PDMS is a popular choice for the use of miniature organs as it is transparent, easily molded and has a high biocompatibility[55]. Later, cell culture medium is added and cell suspensions of the desired cell types are introduced into the previously formed microchannels[57]. The minimal requirements for a microfluidic chip, a single-channel device, are PDMS stamps with only two inlets plus the main channel and one outlet (fig. 5b). This stamp is again, as described previously, bonded to a glass slide[50].

1.11.2 OOACs with mechanical inputs

An emerging field working with OOACs focuses on the implementation of mechanical inputs. Biomechanical cues are crucial for mimicking the physiologic environment of many tissues and organs[17]. In the muscle for example, the implementation of stretching conditions into the experimental setting of the microchip has been shown to positively influence muscle healing progress and outcome after injury. For this purpose, a damage model has been set up in a stretchable (by installation of a 3D-printed stretcher) microfluidic system, simulating natural stretching conditions as observed in muscle tissue *in vivo*. These cyclic stretch-stimuli shortened the overall recovery time and resulted in greater muscle strength, compared to the non-stretched control group[56].

Another experiment including biomechanical stimuli into a biochip set-up, investigated the effect of circumferential stretching of pulmonary artery smooth muscle cells (PASMCs). Using an elastic membrane, circumferential stretching has been simulated at a physiological heartbeat frequency of 80 beats per minute. By addition of this biomechanical stimulus, the proliferation of PASMCs and patient-own PASMCs could be reinforced[57].

Overall, micro engineered cell culture systems, like the organs-on-a-chip, have great potential to establish translatable disease models that reliably predict the *in vivo* behavior of drugs and toxins[13,14]. At the same time, studying underlying pathways and mechanisms would be possible. This would not only be useful in the pharmacologic field but would also be interesting for the chemical and cosmetical industry. The use of biochips could potentially substitute for traditional animal testing approaches in many fields[13].

Given the evidence, that stretching conditions play a vital role affecting various cell types and tissues, the inclusion of biomechanical cues seems inevitable in the construction of adequate *in vitro* disease models. The aim of this thesis is to establish an organ-on-a-chip system for primary equine tenocytes that allows to grow 3D tendon organoids that can be subjected to mechanical inputs in future experiments. Based on these organoids a novel disease model for the investigation of tendinopathies induced by overuse can be investigated in the future. This should provide for a valid alternative to animal testing for pathophysiologic studies and for possible drug screenings.

2. Material & Methods

2.1 Cell bank

For the establishment of a primary equine tenocyte cell bank, the superficial digital flexor tendons (SDFT) of four horses were collected *postmortem*. All horses were euthanized at the university of veterinary medicine Vienna due to reasons unrelated to this study. All samples were labeled with the name of the horse, the date, and tissue type at any timepoint.

The SDFT was dissected from the equine forelimb under sterile conditions by a veterinarian and was immediately transferred to phosphate buffered saline (PBS) to keep it from drying out. In a laminar air flow hood (Safety Cabinet Herasafe KS18, Thermo Fisher Scientific, USA) the tendon was processed further. It was transferred to a sterile petri-dish (Cellstar® Cell Culture Dishes, PS, 100 x 20 mm, with vents, sterile, Greiner Bio-One GmbH, Germany) containing a small amount of PBS, again to prevent drying out. Any layers of tissue adhering to the tendon were removed using a scalpel and forceps. The tendon was cut into small 5 x 5 mm pieces and five to six of these small tendon explants were placed in each well of a 6-well-plate (TC-Plate 6 well, standard, F, Sarstedt, Germany). Per well, approximately 1.5 mL of culture medium were added. To allow cell migration, the tendon explants must touch the bottom of the plate and should not float in the medium. Therefore, if necessary, the volume of the medium added must be adjusted accordingly. The explants were then incubated at 37 °C and 5 % CO_2.

Two times a week, the cell migration progress was examined using a microscope (CKX41, Olympus©, Japan) and medium was changed. For the medium change, the old medium was removed, the explants were carefully washed with 1 mL PBS per well and were then covered with 1.5 mL fresh culture medium. With a cell density of approximately 60 %, the tendon explants were removed using forceps and the plate was re-incubated for another few days. The cells were harvested once the desired cell number was reached. The medium was removed, and the cells were washed with 1 mL of PBS (free from calcium and magnesium) before adding 0.5 mL trypsin to each well. The plate was then incubated for 5 minutes at 37 °C and 5 % CO_2 and viewed with the microscope to check the detachment progress. By addition of 1 mL culture medium, the trypsin was inactivated. The remaining steps of cell harvesting were performed according to 2.2.2.

2.2 General cell culture

Equine tenocytes were cultivated in sterile flasks (TC Flask T175, Stand., Vent. Cap, Sarstedt, Germany) and kept in the incubator (HERAcell 240i, Thermo Scientific, USA) at 37 °C and 5 % CO_2. Culture medium was changed two times a week. All solutions used for cell maintenance and harvesting were prewarmed at 37 °C in a water bath (GFL 1004 water bath, GFL, Germany).

The culture medium (see table 1) was composed of Dulbecco`s Modified Eagle Medium (DMEM; Dulbecco's Modified Eagle Medium, gibco, Life Technologies Europe B.V., Netherlands), 10 % fetal calf serum (FCS; Fetal calf serum, Sigma Aldrich, USA), 1 % Penicillin and Streptomycin (Penicillin-Streptomycin, Sigma Aldrich, USA), and 1 % Amphotericin B (Amphotericin B, Biochrom, England).

Table 1: Culture medium

Ingredients	volume
Dulbecco's Modified Eagle Medium	440mL
Fetal Calf serum	50mL
Penicillin/Streptomycin	5mL
Amphotericin B	5mL

2.2.1 Changing the medium

The old culture medium was removed using serological pipettes (serological pipette, 5ml/10ml/25ml, Sarstedt, Germany). To wash the cells, 10 mL of phosphate buffered saline (PBS; Dulbecco's Phosphate Buffered Saline, gibco, Sigma Aldrich, USA) were added and the flask was waved carefully. Then the PBS was removed, and the cells were covered with 20 mL of fresh medium.

2.2.2 Cell harvesting

Cells were usually harvested at a cell density of approximately 90 %. The medium was removed, and cells were washed with 10 mL PBS free from calcium and magnesium. To detach the cells from the bottom of the flask, 7 mL Trypsin (0.05 % Trypsin-EDTA, gibco, Life Technologies Limited, UK) were added. The flask was lightly waved to make sure all cells are covered before incubating for five minutes. Afterwards the flask was checked with the microscope to verify that all cells detached from the bottom. The flask was tapped

carefully if necessary to facilitate cell detachment. Trypsin was inactivated by addition of 7 mL culture medium. The whole solution was then transferred to a prelabeled tube (15 mL tube, 120 x 17 mm, PP, Sarstedt, Germany) and centrifuged for 5 minutes at 400 g at 20 °C (ROTANTA 460 R, Andreas Hettich, Germany). After centrifugation a cell pellet is visible. The supernatant is removed and the cells are resuspended in 10 mL PBS and centrifuged (5 min, 400 g, 20 °C) again to wash the cells. Again, a pellet is formed, and the supernatant is removed completely.

2.2.3 Cell counting

To prepare the cells for counting, the harvested tenocytes (compare 2.2.2) were resuspended in 5 mL culture medium. The solution was mixed well before transferring 10 µL to an Eppendorf tube (1.5 mL SafeSeal tube, Sarstedt, Germany). For cell staining, 10 µL of trypan blue (Trypan Blue Stain 0,4%, Invitrogen, USA) were added and again, the solution was mixed well. A cell counting chamber slide (Countess cell counting chamber slides, Invitrogen, USA) was prepared and 10 µL of the cell-trypan blue mix were filled into each of the two counting chambers. The slide was then inserted into the automated cell counter (Countess II FL Automated Cell Counter, Life Technologies, USA) and both chambers were counted. The device measures the cell concentration per mL and values for cell viability (proportion of live and dead cells).

2.2.4 Cell freezing

The freezing procedure is time sensitive as the cells should not be exposed to the DMSO-containing freezing medium any longer than necessary. Cells were harvested as described above (2.2.2 cell harvesting) and the cell pellet was resuspended in 4 mL freezing medium, which is composed of FCS with 10 % Dimethyl sulfoxide (DMSO; Dimethyl sulfoxide, Sigma Aldrich, USA). 1 mL of the cell suspension were then added to four prelabeled cryotubes (CryoPure tube 1.8 mL yellow, Sarstedt, Germany) which were immediately cooled in a freezing container (Nalgene Cryo 1 °C Freezing Container Mr. Frosty, Sigma Aldrich, USA), which reduces the temperature by 1 °C per minute. The cells were then kept at -80 °C for 24 hours before storing them at -150 °C.

2.2.5 Cell thawing

1 mL of prewarmed medium was added to the cryotube, which was handheld to speed up thawing. As soon as the cell solution melted, the content of the cryotube was transferred to a 15 mL tube and 8 mL of culture medium were added. The tube was centrifuged (5 min, 400 g, 20 °C) and the supernatant was discarded. The cell pellet was washed with PBS for two times. Afterwards, the cells were resuspended with medium, transferred to a cell culture flask, and were incubated at 37 °C and 5 % CO_2.

2.3 Development of the Biochip

The microfluidic chips were designed based on the size of a standard slide (26 mm x 76 mm) and are composed of 0.5 mm thick layers of polydimethylsiloxane (PDMS) foil. The designs of each layer were created with the software Autodesk AutoCAD (computer-aided design) 2020 (autodesk.com/products/autocad/, 08.10.2020). The detailed designs are to be found in 3.1 Development and design of the biochip.

2.3.1 Manufacture of the biochip

The individual layers for the biochip were plotted (Microfab Roland Plotter CAMM-1 GS-24, Roland DG Corporation, Germany) on a 0.5 mm PDMS foil (SuperClear Silicone Sheet 5HT6240GK 0.5 mm, MVQ Silicones GmBH, Germany) with a carbide blade (Cemented Carbide blade ZEC-U5032, Roland DG Corporation, Germany). The resulting structures which form the chambers and channels were removed using forceps. To join individual layers, they were plasma treated for two minutes (Plasma Cleaner PDC-002-CE, Harrick Plasma Inc, USA) before bonding. After each layer, the chip was wedged between two glass slides to ensure proper bonding and was then put into an oven (Drying chamber ED 53, Binder, Germany) at 80 °C for at least 15 minutes before adding the next layer. After assembly of all layers, the chip was kept at 80 °C for additional 30 minutes, whenever possible the chip was left incubated longer or even overnight.

For microfluidic chips that were not mechanically stimulated, a glass slide (Microscope Slides, Marienfeld, Germany) was added to the bottom to increase stability and ease

handling. Mechanically strained chips were provided with additional top and bottom PDMS layers to avoid excessive deformation during strain application.

2.3.2 Chip preparation & loading

Before usage, all chips were UV treated for at least one hour to sterilize them. Prior to loading, all chambers, wells and channels were coated with lipidure (Lipidure® CM5206, NOF Europe, Germany) if not stated otherwise. 1 g lipidure was dissolved in 200 mL ethanol to create a 0.5 % solution and was then sterile filtered (Easy strainer, 100 µm, Greiner bio-one, Austria) before use. All microfluidic channels and chambers were filled with lipidure solution. After one minute, the solution was entirely removed, and the system was air-dried at room temperature.

To load the chip with a cell-containing hydrogel, at least 20 µL surplus of cell-hydrogel mixture were taken up with the pipette. Therefore, some material remained in the tip when filling the main chamber, to avoid bubble formation.

2.4 Examination of cell viability

2.4.1 FDA/PI Assay

To evaluate cell viability, a fluorescence-based live-dead staining assay using fluorescein diacetate (FDA; Fluorescein diacetate, Lot#MKBR3002V, Sigma Aldrich, USA) and propidium iodide (PI; Propidium iodide, Lot#MKCB0899V, Sigma Aldrich, USA) was used. Viable cells take up FDA and metabolize it to fluorescein (green). PI is a nucleus staining dye that intercalates with DNA. In a viable cell, propidium iodide is unable to pass the cellular membrane hence it can easily enter through the dysfunctional membrane areas of dead cells. PI stains dead cells red.

3D cell constructs were transferred to the wells of a 24-well-plate (TC-Plate 24 well, standard, F, Sarstedt, Germany). The staining solution was freshly prepared using 5 mL culture medium (without FCS), 8 µL FDA (5 mg/mL) and 50 µL PI (2 mg/mL) and was kept protected from light. To each construct, 0.5 mL staining solution were added, and the plate was incubated for 5 minutes at room temperature in the dark. Then, the 3D constructs were evaluated with fluorescence microscopy (EVOS FL Auto, life technologies, USA).

2.4.2 MTT Assay

The CellTiter 96® AQ_{ueous} One Solution Cell Proliferation Assay combines a tetrazolium compound [3-(4,5-dimethylthiazol-2-yl)-5-(3-carboxymethoxyphenyl)-2-(4-sulfophenyl)-2H-tetrazolium, inner salt; MTS] and an electron coupling reagent (phenazine ethosulfate; PES) used to indirectly determine the presence of viable cells based on their proliferation activity. Metabolically active cells reduce the contained tetrazolium compound to a colored formazan. For a 3D hydrogel containing living cells, this results in a color change of the whole construct to purple after one hour of incubation at 37 °C and 5 % CO_2. For a cell-containing hydrogel of approximately 80 to 100 µL total volume, 100 µL culture medium were mixed with 20 µL CellTiter 96® AQ_{ueous} One Solution reagent (CellTiter 96® AQ_{ueous} One Solution reagent, LOT 0000282592, Promega, USA) for staining.

2.5 RNA isolation and qPCR

2.5.1 RNA isolation & concentration

The workspace was precleaned with RNase away spray (RNase AWAY, Molecular Bio Products, USA). A solution containing 1 mL trizole (TRIzol LS Reagent, Invitrogen, USA) and 10 µL 2-mercaptoethanol (2-Mercaptoethanol, Sigma Aldrich, USA) per sample was prepared and 1 mL of solution was added to each sample before mixing carefully. In case of 3D constructs, the collagen hydrogel was retrieved from the microfluidic chip using a scalpel and tweezers. The samples were vortexed (RS-VA 10, Phoenix Instruments, Germany) for approximately 5 minutes until it dissolved. Then, the solved sample was transferred to a 2 mL Eppendorf tube (2 mL SafeSeal tube, Sarstedt, Germany) and 200 µL chloroform (Chloroform, Sigma Aldrich, USA) were added. The solution was incubated for 5 minutes at room temperature and mixed occasionally, before centrifuging it (Fisher AccuSpin Micro17R, Thermo Fisher, USA) for 15 minutes at 13000 rpm and 4 °C. Three phases should then be visible: an aqueous upper phase that contains the RNA, an intermediate phase containing the DNA and an organic phase at the bottom of the tube, which contains proteins and lipids. Approximately 200 µL of clear upper phase were transferred to a fresh Eppendorf tube and 200 µL of DEPC water (DEPC-Treated Water, Ambion, USA) and 320 µL isopropanol (Isopropanol 99.5%, Acros Organics, USA)

were added. After adding 1 µL glycoblue (GycoBlue Coprecipitant, Invitrogen, USA), the samples were vortexed and incubated for 20 minutes on ice. After the incubation period, the samples were centrifuged at 13000 rpm for 30 minutes at 4 °C. A bluish RNA pellet becomes visible which is adherent to the bottom of the tube. The supernatant was removed, and the sample was washed two times with 500 µL of 75 % EtOH (14000 rpm, 5 minutes, 4 °C). Again, the supernatant was removed with a pipette and the remaining EtOH was evaporated at room temperature. To dissolve the RNA pellet, 20 µL of RNase free water (Nuclease-Free Water, Invitrogen, USA) were added (without pipetting).

To get rid of any remaining DNA, DNA digestion reagents (see table 2) were added and the samples were incubated at 37 °C for 30 minutes (Thermocell cooling and heating block, BIOER, China).

Table 2: Reagents for DNA digestion

Reagent	volume (per sample)
10x DNase Buffer	3 µL
rDNase	1 µL
Nuclease-free water	6 µL

Then, 3 µL of DNase inactivation reagent (DNase Inactivation Reagent, Invitrogen, USA) were added and the sample was mixed well. After 2 minutes of incubation at room temperature, the samples were centrifuged for 2 minutes at 13000 rpm. Two phases become visible and the clear upper phase, which contains the RNA, was transferred to a fresh tube and kept on ice. The RNA concentration was measured with a nanophotometer (NanoPhotometer N60, Implen, Germany). In case for low RNA yields, the RNA concentration was determined by Qubit RNA HS assay kit (Qubit RNA high selectivity Kit, Invitrogen, USA) and Qubit fluorometer (Qubit 4 fluorometer, Invitrogen, Singapore). After quantification, the isolated RNA was stored at -80 °C until used for qPCR.

2.5.2 Primers

All primers (see table 3) were designed by Sinan Gültekin PhD and ordered as lyophilizate from Microsynth (Switzerland). They were resolved to a stock concentration of 100 µM in nuclease-free water and stored at -20 °C. Primer dilutions for quantitative PCR were made of 10 µL forward primer and 10 µL reverse primer diluted in 80 µL nuclease-free water.

Table 3: Primers for qPCR

Gene	Abbreviation	Forward primer	Reverse Primer
Collagen type I alpha 2	Col1a2	TCCATCTGGAGAGCCTGGTA	CACCTGGTAGACCACGTTCA
Decorin	DCN	ACATAACCACCATCCCTCCA	CTCAGGCTAGCTGCATCAAC
Glycerinaldehyd-3-phosphat-Dehydrogenase	GAPDH	GTTTGTGATGGGCGTGAAC	GATGCCAAAGTGGTCATGG
Interleukin 6	IL-6	ATGGCAGAAAAAGACGGATG	GGGTCAGGGGTGGTTACTTC
Matrix-metalloproteinase-13	MMP13	TGGTCCAGGAGATGAAGACC	GATGGCATCAAGGGATAAGG
Mohawk	Mkx	TTACAAGCACCGTGACAACC	AAGCCGACGTCTTGCATTAG
Peptidylprolyl Isomerase A	PPIA	ACCCTACCGTGTTCTTCGAC	ATCCTTTCTCCCCAGTGCTC
Acidic ribosomal phosphoprotein P0 (36B4)	Rplp0	TGCATTCTCGCTTCCTGGAG	TCCACAGACAAAGCCAGGAC
Scleraxis	Scx	CCCAGACCCACTGGAACTT	ACACAAGATGCCAGCACGTA
Tenascin C	TNC	ACCTCAGAGAAGGGCAGACA	CACCGTGAGGTTTTCCAGTT
18S ribosomal RNA	18S	TTTCGATGGTAGTCGCTGTG	CTTGGATGTGGTAGCCGTTT

2.5.3 Quantitative PCR

For each quantitative PCR (qPCR) reaction, 4 ng RNA (2 ng/µL) were used per sample. The total reaction volume amounted to 10 µL (2 µL sample and 8 µL master mix) and was pipetted by a pipetting robot (epMotion 5075, Eppendorf, Germany). The master mix contained nuclease-free water, the primer dilution (forward and reverse primer) and the polymerase (compare table 4). Samples were analyzed in duplicates and transcript levels were normalized to the levels of the housekeeping genes (GAPDH, PPIA, Rplp0, 18S) based on the $2^{-\Delta\Delta C_t}$ (Livak) method. A negative control was included for each gene.

Table 4: Master mix for qPCR

Reagent	volume (per sample)
Enzyme	2.5 µL
Forward primer	0.4 µL
Reverse primer	0.4 µL
Nuclease-free water	4.7 µL

For cDNA generation and for the ensuing qPCR, RevTrans qPCR One-step EvaGreen kit (Bio&Sell, Germany) was used. The samples were incubated for 15 minutes at 50 °C for cDNA synthesis. For the qPCR reaction, they were heated to 95 °C for 5 minutes, to 95 °C for 20 seconds, to 58 °C for 30 seconds and to 72 °C for 20 seconds. In the subsequent melting curve stage, samples were heated to 95 °C for 15 seconds, to 60 °C for one minute and to 95 °C for another 15 seconds. The software used for analysis was QuantStudio real-time PCR software v1.3 (QuantStudio Real-Time PCR software, Applied Biosystems, USA).

2.6 Experimental set-up

2.6.1 Pilot experiment 1 – most suitable hydrogel

To examine whether collagen or fibrin is better for 3D cultivation of equine tenocytes, microfluidic systems (cigar design) were loaded in duplicates comparing three different cell numbers for each hydrogel. Cell numbers were 600 cells per tendon, 1200 cells per tendon and 2400 cells per tendon. The concentration of the fibrin hydrogel (Fibrinogen from human plasma, Lot#SLCD3003, Sigma Aldrich, USA) was 2.5 mg/mL fibrin. The collagen (PureCol EZ Gel solution, Lot#SLCG2035, Sigma Aldrich, USA) concentration was 2.2 mg/mL.

2.6.1.1 Preparation of the collagen hydrogel

To prepare the collagen-cell-mixture, the total volume of hydrogel needed was determined and the proportion of collagen and cells suspended in medium was calculated. For example, for a total volume of 500 µL hydrogel (with a collagen concentration of 4 mg/mL): 400 µl of collagen (5 mg/mL) were mixed with 100 µL cells suspension.

For the primary preparation of the cell suspension, cells were trypsinized and counted as described before. The counted cell number in per mL was converted to the absolute cell number and the amount of cells needed (dependent on the number of microfluidic systems) was determined. The cells were centrifuged, and the cell pellet was diluted accordingly.

All pipetting steps involving collagen were carried out on ice to avoid premature collagen polymerization. Special attention was paid to avoid bubble formation.

2.6.1.2 Preparation of the fibrin hydrogel

The amount of fibrin powder needed was calculated, weighted, and solubilized in prewarmed PBS to mix a stock solultion. The hydrogel solution was then sterile filtered (Millex®GP Filter unit 0.22 µm, Merck Millipore Ltd., Ireland) using a syringe (Injekt® Luer Solo 20 mL, B. Braun Melsungen AG, Germany) and mixed with the cell-medium

suspension to a final concentration of 2.5 mg/mL fibrin. As the fibrin gel is more viscous then the collagen mixture, the pipette tips were cut to ease pipetting when necessary.

2.6.2 Pilot experiment 2 – collagen concentration

To ensure optimal collagen polymerization, three concentrations of collagen were tested: 2.2 mg/mL, 3.33 mg/mL and 4 mg/mL. To achieve the different concentrations the collagen stock solution of 5 mg/mL was diluted accordingly using DMEM culture medium. For each of the three concentrations, 8 drops containing 80 µL of hydrogel were pipetted on a 24-well-plate. Medium was added either after 90 or 120 minutes. The plate was cultivated for 7 days.

2.6.3 Pilot experiment 3 – tendon on a chip

To examine tendon formation on the chip, two different cell numbers were seeded in triplicates using a 4 mg/mL collagen hydrogel and an oval chip design. Cell numbers tested were 1200 cells per tendon and 80000 cells per tendon.

Additionally, duplicates of a biochip containing 30000 tenocytes in a 4 mg/mL collagen hydrogel were loaded. All Chips were cultivated for two weeks. One of the microfluidic systems containing 80000 cells was harvested for histological evaluation. The PDMS layers covering the main chamber were carefully removed using a scalpel and the organoid was retrieved with forceps. To conserve the elongated tendon shape, the tendon was fixed to a wooden spatula and was kept in formol (formaldehyde solution 4%, buffered, pH 6.9, Sigma Aldrich, Germany) until histological processing.

2.6.4 Pilot experiment 4 – hydrogel rigidity & permeability

To evaluate the rigidity of the hydrogel in a chip-like set up and size ratio, molds were prepared using liquid silicone (SYLGARD™ 184 Silicone Elastomer, Dow Chemical Company, USA) and a negative 3D print (design source: Gil Oreff). 40.5 mL of base reagent (DOWSIL 184 silicone elastomer base) were transferred into a 50 mL tube (50mL

tube, 114x28mm, PP, Sarstedt, Germany) and 4.5 mL of curing agent (DOWSIL 184 silicone elastomer curing agent) were added. The 5 mL pipette was left in the tube and was used to stir for 5 minutes. The mixture was then poured into the negative mold and was allowed to settle, before the mold was repeatedly smacked on the table to get rid of remaining bubbles. It was then placed aside for two days to let it dry at room temperature. When the silicone hardened, it was removed from the mold using a flat spatula and was autoclaved before use. A single silicone mold of 83 mm diameter carried 31 pits of 10 mm length and 3 mm width (see fig. 6).

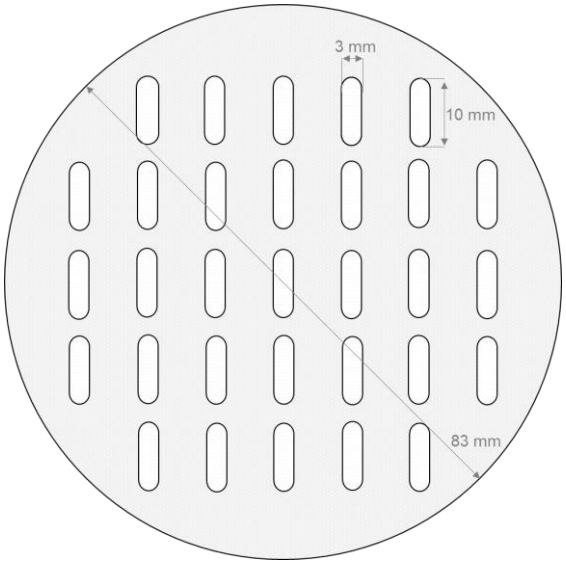

Figure 6: Schematic representation of the silicon mold *with a diameter of 83 mm. Pit size: length = 10 mm and width = 3 mm*

The rigidity of 2.2 mg/mL, 3.33 mg/mL and 4 mg/mL collagen gels was determined. A sterilized silicone mold was transferred to a 100 x 20 mm sterile petri-dish. Collagen hydrogels of the respective concentrations were prepared without cells and triplicates were loaded into the silicone pits (fig. 7: A). The dish was then placed in the incubator for approximately one hour.

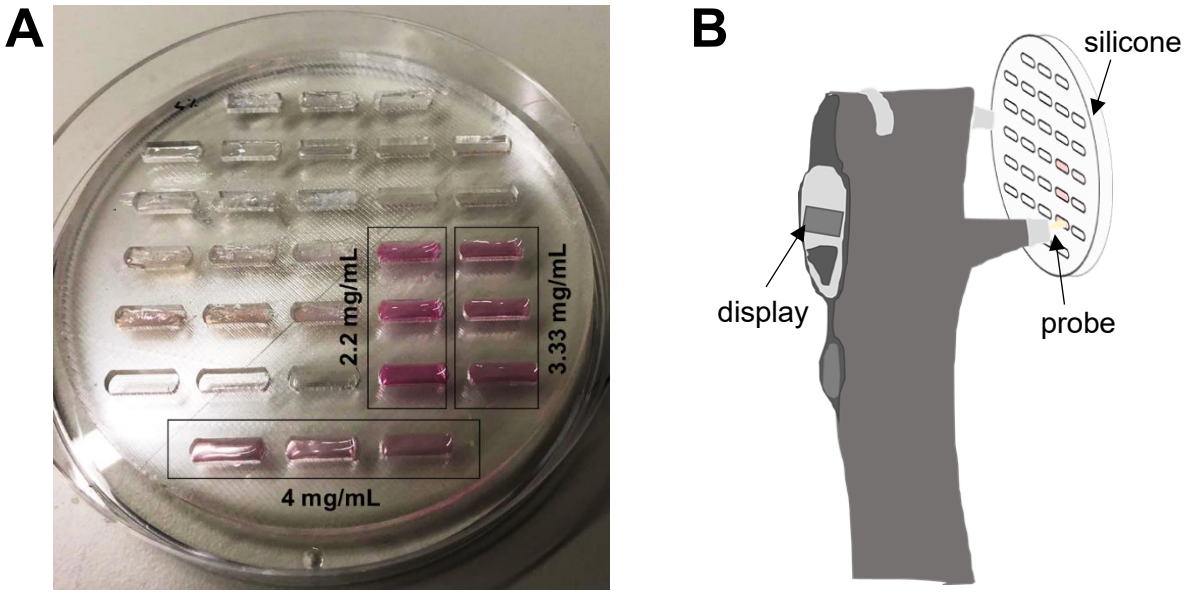

Figure 7: Hydrogel rigidity measuring (A) *Picture of the silicone loaded with triplicates of 2.2 mg/mL, 3.33 mg/mL and 4 mg/mL collagen hydrogel* ***(B)*** *Illustration of rigidity measurement using the iCare TonoVet*

Rigidity measurements were carried out using a tonometer (TonoVet Tonopen XL, iCare, Finland), which is normally used to determine the intraocular pressure of animals in a clinical setting. Using a rebound measuring principle, a light weight probe makes momentary contact with the surface that should be evaluated and measures the resistance 6 times[58]. The highest and lowest value measured is discarded. Using calibration curves, the software takes the remaining four measurements to calculate the rigidity in mmHg[58]. The device must be held upright (vertically), as the probe may slip out otherwise, in a distance of 4 to 8 mm to the surface of interest (fig. 7: B).

Further, the permeability of 2.2 mg/mL, 3.33 mg/mL and 4 mg/mL collagen gels was evaluated on-the-chip. Hydrogels of the respective concentrations were loaded and allowed to polymerize at 37 °C for 45 minutes. Using the function “time lapse” of the EVOS FL Auto microscope and a GFP filter, the diffusion of a 1 µg/mL fluorescein solution into the hydrogel was tracked. Pictures were taken every three minutes over a time period of 60 minutes. Using the software Image J – Fiji[59] and the function “Image > Adjust > Color Threshold” the green fluorescent area in the single pictures was made clearer and converted to white using the following settings: Hue 94 and 250; Saturation 255 and 255;

Brightness 26 and 25; Threshold method - default; Threshold color - white; Color space – HSB. Using lines, the progression of the fluorescent area was measured, comparing the pictures of 0, 27 and 60 minutes after addition of fluorescein (fig. 8)

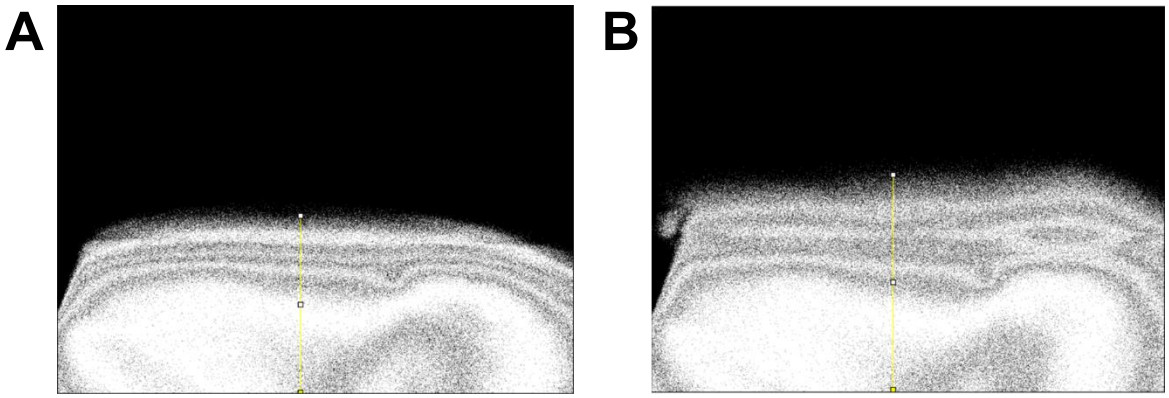

Figure 8: Fluorescein diffusion. *Fiji picture with adjusted Color Threshold at time point 1 (A) and 10 (B) after addition of fluorescein.*

The measurements were converted to µm and the diffusion coefficient in µm per minute was calculated. For each hydrogel concentration 9 measurements were taken into account, with the highest and lowest value being discarded. The mean diffusion coefficient was calculated from the remaining 7 values.

2.6.5 Pilot experiment 5 – cell condensation and survival

1200 equine tenocytes per 80 µL were seeded in 3.33 mg/mL and 4 mg/mL of collagen on a 24-well-plate. Two drops of pure collagen (5 mg/mL) were pipetted as a control. On the bottom of the plate, the size of each drop was marked to track the initial drop size and visualize shrinkage- The plate was cultivated for 14 days.

To check whether the cells survived in the collagen construct, the hydrogel drops were transferred to a fresh plate and FDA/PI and MTT assays were carried out as described before.

2.6.6 Pilot experiment 6 – tendon defect

Two chips of the oval design were loaded with a 4 mg/mL collagen hydrogel and 80000 equine tenocytes. After 14 days of cultivation, one of the tendon-organoids formed was mechanically injured using a biopsy punch (biopsy punch 0.3 mm, ProSciTech, Australia) puncturing the PDMS layers above the main chamber and the tendon. The other tendon was injured twice, using the 0.3 mm biopsy punch and a syringe (Needle 0.6 x 30 mm, Terumo Europe N.V., Belgium). The injured organoids were cultivated for additional 14 days. In total, the cultivation time of the biochips was 28 days.

2.6.7 Pilot experiment 7 – "pin variation"

To evaluate whether continuous or non-continuous PDMS pins are more suitable for the cultivation and mechanic stimulation of tendons-on-a-chip, three variations of pin designs were tested. The continuous design in which both PDMS pins are connected with the top layer (fig. 9: B) of the main chamber, a semi-continuous pin design with only one pin connected to the top layer (fig. 9: C), and a non-continuous pin design where none of the two pins reaches the top layer of the main chamber (fig. 9: D).

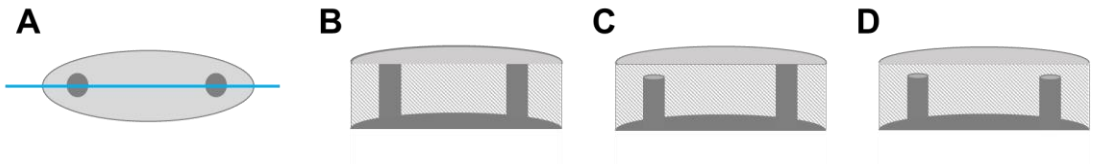

Figure 9: Pin variation. ***(A)*** *Section trough the main chamber for lateral view of B, C and D* ***(B)*** *Continuous design: both PDMS pins connected to the ceiling* ***(C)*** *Semi-continuous design: only one PDMS pin connected to the top layer* ***(D)*** *Non-continuous design: none of the PDMS pins reaches the ceiling*

Three microfluidic systems of the oval design with the three different variations of PDMS pins were used. The chips were loaded with a 4 mg/mL collagen hydrogel containing 80000 equine tenocytes and cultured for 14 days.

2.6.8 Pilot experiment 8 – characterization of tendon strain

For the application of mechanical strain to the tendon-on-a-chip, a template traction was built of LEGO® (fig. 10).

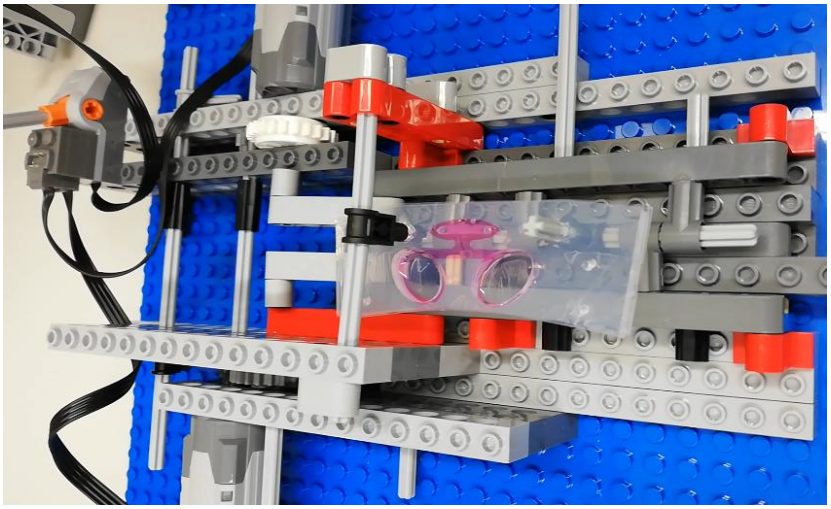

***Figure 10: Lego® template** for the implementation of biomechanical strain to the microfluidic system*

The device allows for the implementation of dynamic uniaxial strain, increasing the pin to pin distance from 9 mm to approximately 11 mm at a frequency of 1.2 Hz, and is powered by two LEGO® engines (LEGO® Technic power functions engine M, LEGO System A/S, Denmark).

To mount the biochip on the LEGO® construct for mechanic stimulation, holes of 3 mm diameter were added to the oval chip design at a distance of 30 mm (see fig. 11: A) to create the mechanic design. Additionally, to increase the stability of the microfluidic system, four of the chips were bonded to a slightly shifted glass slide that would only cover the area of the medium wells (see fig. 11: B). For the duration of the mechanic straining, most of the medium was removed from the reservoirs to avoid spilling out.

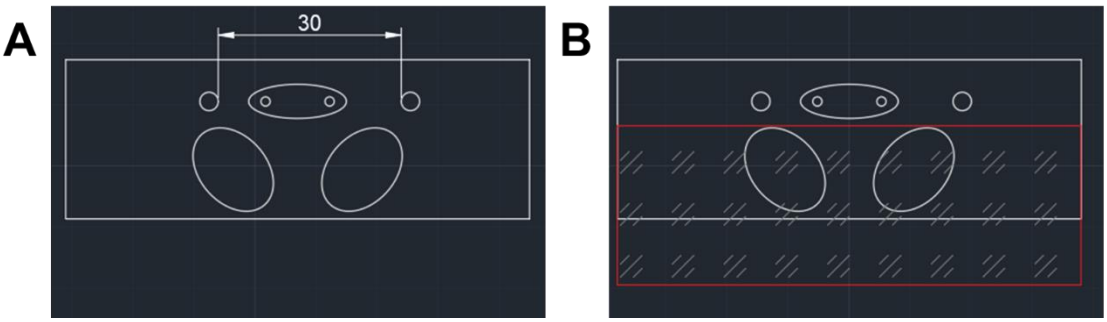

Figure 11: Design modifications for mechanic stimulation (A) *holes of 3 mm in diameter were added besides the main chamber in a distance of 30 mm* ***(B)*** *slightly shifted glass slides (red) were bonded to the bottom layer of the microfluidic system to increase stability*

To determine the deflection of single cells in the construct, 10 microfluidic chips of the oval design were loaded with a 4 mg/mL collagen hydrogel and 80000 cells. Additionally, 0.5 % of auto-fluorescent beads (Fluoro-Max green fluorescent polymer microspheres 9.9 µm, Thermo Fisher, USA) were mixed to the cell suspension. To examine whether the applied strain is directly transmitted to the hydrogel and the tenocytes in the construct, the deflection of green fluorescent particles embedded in the tendon-like structure was measured for 5 microfluidic chips. Videos (VLC media Player – version 3.0.12) and fluorescence pictures were taken using EVOS FL Auto (GFP filter and 4x magnification) in strained and relaxed condition. Three areas of the tendon-like structure were investigated (fig. 12): origin, center and tail.

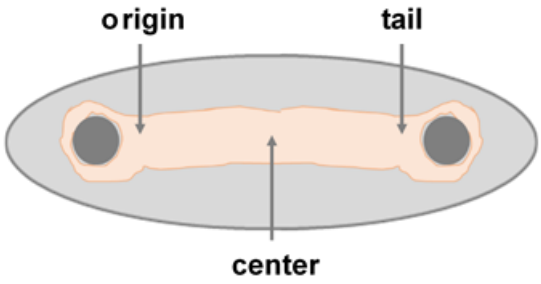

Figure 12: Schematic representation of measurement areas*: origin, center, and tail of the tendon-like structure*

2.6.9 Mechanical tendon stimulation on-a-chip

To evaluate the influence of mechanical training on tendons-on-a-chip, twelve chips of the mechanic design (including two 3 mm holes on either side of the main chamber) containing a 4 mg/mL collagen hydrogel with 80000 tenocytes of three different donors were prepared. Cells of each donor were used for four microfluidic chips: two for mechanic stimulation and two as a control. Mechanical stimulation was started on day 7 post loading of the chip, after a microtendon had formed through contraction of the hydrogel. Dynamic uniaxial strain was applied using the LEGO® construct for 15 minutes once daily for 14 days, increasing the pin to pin distance from 9 mm to approximately 11 mm, which would correspond to around 22 % of strain, at a frequency of 1.2 Hz (at room temperature).

On the fourth day of the biomechanical stimulation, the LEGO® engines failed to stretch the microfluidic chips. To bypass the problem, all movable parts were oiled (Aesculap shear oil, Aesculap, Germany) to reduce friction, the engines were cooled with ice packs and were supported manually using a crank handle if necessary. On day 6, the engines could no longer power the system, necessitating a complete switch to manual mechanical stimulation. The stimulation remained the same for all samples.

2.6.10 Tendon inflammation on-a-chip

To compare different tendinopathy-like states on-the-chip, microfluidic systems were divided into four treatment groups: healthy, healthy injured, inflamed, inflamed injured. The group of “healthy” biochips did not receive any special processing and served as control. To mimic the pathology of tendinosis, “healthy injured” biochips were mechanically injured using a biopsy punch. A tendinitis was aimed to be mimicked using culture medium containing the inflammatory factors TNF-α and IL-1β. For the “inflamed injured” group the tendinopathic state induced was a hybridization of tendinosis and tendinitis by combining the use of inflammatory medium with a mechanical injury.

Tenocytes of three different donors and a total of 32 microfluidic chips were used. Twelve chips of Donor 1, eight of Donor 2 and twelve of Donor 3. Treatment groups were healthy, healthy with injury, inflamed and inflamed with injury. Chips of the group “healthy” were loaded with healthy tenocytes. “Inflamed” samples were cultivated with inflammation medium instead of the normal medium. Inflammation medium (see table 6) contains

10 ng/mL of the inflammatory mediators tumor necrosis factor alpha (TNF-α; rh TNF-alpha 10 µg, LOT 354650, ImmunoTools, Germany) and interleukin-1 beta (IL-1β; IL-1beta/IL1F2, 10 µg, LOT 354600, ImmunoTools, Germany). Therefore, 5 µL TNF-α and 5 µL IL-1β are added to 50 mL of culture media.

The samples “with injury” were either cultivated with normal medium (healthy with injury) or with inflammation medium (inflamed with injury). In order to mimic an injury, each tendon of this group was injured with a 0.3 mm biopsy punch.

As it was not clear whether the tendon-like structures would survive for 14 days, half of the microfluidic chips (6) of Donor 1 were harvested after 7 days. The other half was harvested after 14 days.

For Donor 2 and 3, all microfluidic chips were cultivated for 14 days prior to harvest. Four tendon-like structures of Donor 3, one per group, were set aside for histologic evaluation. The tendons were transferred to a wooden spatula and kept in formol (4%) until further processing. All other samples were snap-frozen for RNA-extraction and qPCR.

2.7 Statistical analysis

For the statistical analysis and data visualization the software GraphPad Prism (version 5.04), R-Studio (R version 4.0.3), and ImageJ – Fiji (version 2.1.1) were used. The significance cut-off for statistical analysis was set to 0.05. Significance levels were determined using an unpaired t-test with two-tailed p-value and were shown as “*” for $p < 0.05$, ”**” for $p < 0.01$, ”***” for $p < 0.001$ and ”****” for $p < 0.0001$.

3. Results

3.1 Development and design of the biochip

3.1.1 Design 1: “cigar”

The “cigar” design (fig. 13: A) is characterized by a main chamber that is formed like a cigar and has integrated PDMS pins. It holds approximately 70 µL and has one central inlet with a diameter of 1 mm. The length of the main chamber is 9 mm, the pin to pin distance is 4.5 mm and the width of the chamber is 3 mm. The cell loaded hydrogel which is cultured in the main chamber is supplied with medium by a channel that is connected to two roundish medium reservoirs. The pins, which are supposed to serve as anchoring posts for the tendon, were designed in three different sizes: 1 mm, 1.25 mm and 1.5 mm. During manufacture of the microfluidic systems, it turned out that small diameters of pins are not always cut properly by the plotter and that their handling and correct placement is very difficult. Therefore, the final cigar design had only pins of 1.5 mm diameter.

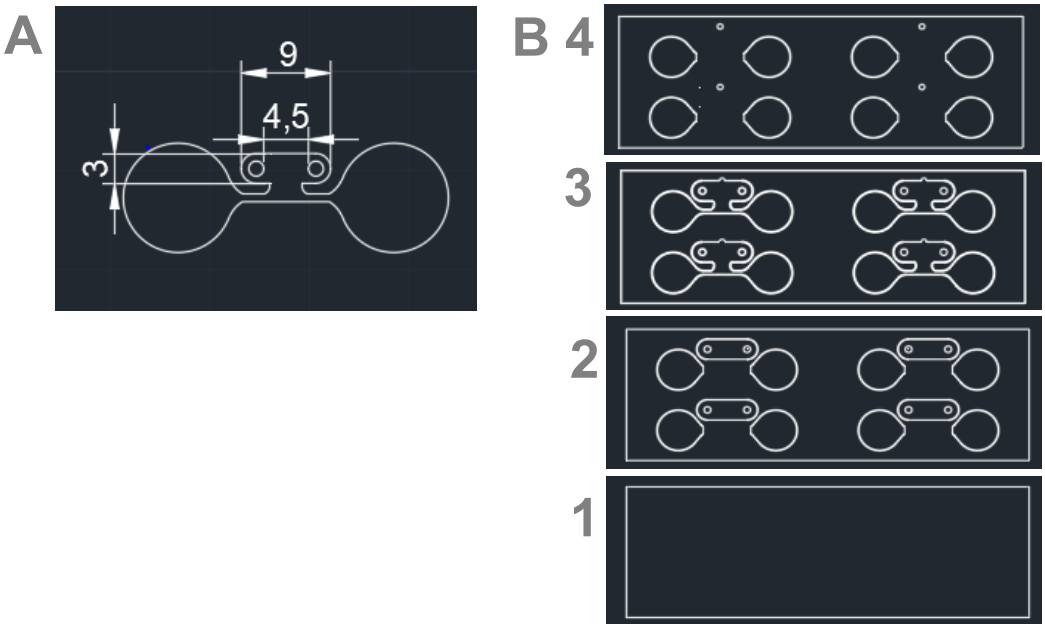

Figure 13: Cigar shaped design. (A) *Dimensions of the main Chamber: Space between the pins = 4.5 mm; chamber length = 9 mm; chamber width = 3 mm.* ***(B)*** *All individual layers of the biochip: (4) top layer (3) channel layer (2) chamber base layer (1) basement layer. All layers are 26 mm x 76 mm.*

The microfluidic chip is made of 9 individual layers that are bonded together (see fig. 13: B). The basement layer (B1) has no cut-out structures and is bonded to a glass slide. The other layers have cut-outs to form the medium reservoirs, main chamber and medium channels. The next layer, the chamber base (B2) is the bottom of the main culture chamber and the medium wells. The channel layer (B3) comprises the medium wells and main chamber and connects the main chamber to the medium wells. Three of those layers are used. The top layer (B4), of which four are bonded to the chip, serves as ceiling for the main chamber leaving only a small inlet open and increases the volume of the medium wells.

3.1.2 Design 2: “oval”

The “oval” design (fig. 14: A) is characterized by an oval main chamber with integrated PDMS pins that are 1.5 mm in diameter. The main chamber has a volume of approximately 100 µL and has three inlets: the main inlet is placed in the center and two additional ones are left and right of the two pins. Each inlet has a diameter of 1 mm. The entire length of the main chamber is 16 mm, the pin to pin distance is 9 mm and the width of the chamber is approximately 5.3 mm at the thickest part. The chamber is connected to two oval medium reservoirs by a medium channel.

The biochip of the oval design consists of 6 PDMS layers (fig.14: B). The basement layer (B1) has no cut-out structures and is bonded to a glass slide. The other layers have cut-outs to form the medium reservoirs, main chamber and medium channels. The chamber base layer (B2), is the bottom of the main chamber and the medium wells. Two channel layers (B3) which include (in addition to the medium reservoirs and the main chamber) a channel that connects the medium reservoirs with the main chamber are added. The last type of layer, the top layer (B4), is used two times and seals the main chamber leaving only the three inlets open. Further, it also increases the volume of the medium wells.

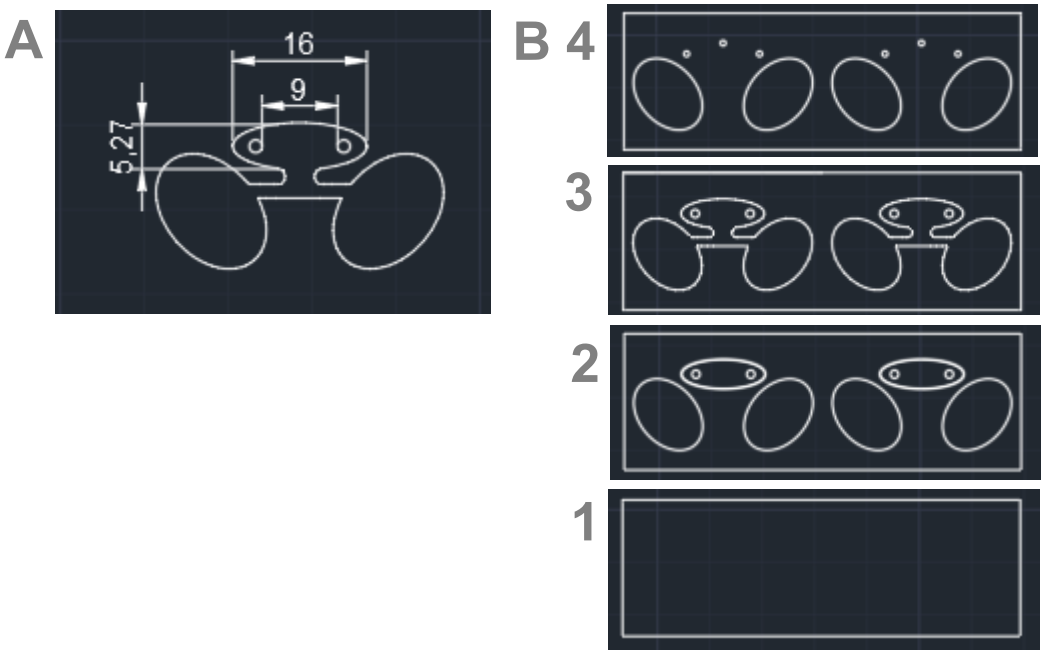

Figure 14:* Oval design.** ***(A) *Dimensions of the main Chamber: Space between the pins = 9 mm; chamber length = 16 mm; chamber width = 5.27 mm.* ***(B)*** *All individual layers of the biochip: (4) top layer (3) channel layer (2) chamber base layer (1) basement layer. All layers are 26 mm x 76 mm.*

3.1.3 Design 2: "mechanic"

The mechanic design (fig. 15: A) shares the basic design with the oval biochip. The dimensions of the main chamber are the same as for the oval design, but the main chamber as well as the medium channel was shifted upwards to increase the distance to the medium wells. The size of the medium channel was increased.

The mechanic chip is made of 9 layers that are bonded together (see fig. 15: B). Three continuous PDMS layers, the basement layers (B1) are bonded together. The chamber base (B2) is the bottom of the main culture chamber and the medium wells. The channel layer (B3) is used twice for each chip and comprises the medium wells and main chamber. The top layer (B4), of which three are bonded to the chip, serves as ceiling for the main chamber leaving only a small inlet open and increases the volume of the medium wells.

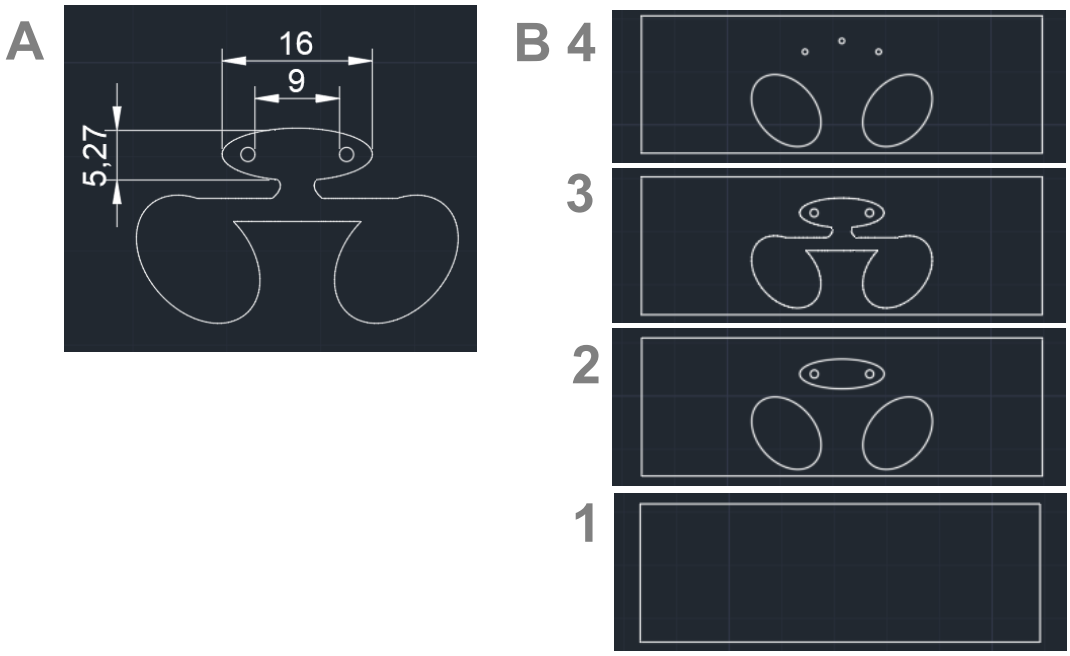

Figure 15: **Mechanic design.** ***(A)*** *Main chamber and channel shifted upwards to create distance to the medium wells. Dimensions of the main Chamber: Space between the pins = 9 mm; chamber length = 16 mm; chamber width = 5.27 mm.* ***(B)*** *All individual layers of the mechanic biochip: (4) top layer (3) channel layer (2) chamber base layer (1) basement layer. All layers are 26 mm x 76 mm.*

3.2 Pilot experiment 1 – most suitable hydrogel

To examine the most suitable hydrogel, collagen and fibrin hydrogels containing three different cell numbers were tested. There were major difficulties to load the main chamber of microfluidic chips with the cigar shaped design. The hydrogel did not fill the chamber evenly, eventually floated into the medium channel, or contained air inclusions. All the 2.5 mg/mL fibrin hydrogels either dissolved or floated into the medium channels. A comparison of the different cell numbers that were seeded in fibrin hydrogels was therefore impossible. The 2.2 mg/mL collagen hydrogels remained in the main chamber, but except for a single chip no tendon-like structures were formed after 10 days. Chambers loaded with 600 cells displayed very low cell density, while those with 1200 or 2400 cells showed a higher cell density. The hydrogel of some of the 1200 cells containing chips slightly condensed after two days of cultivation (see fig. 16).

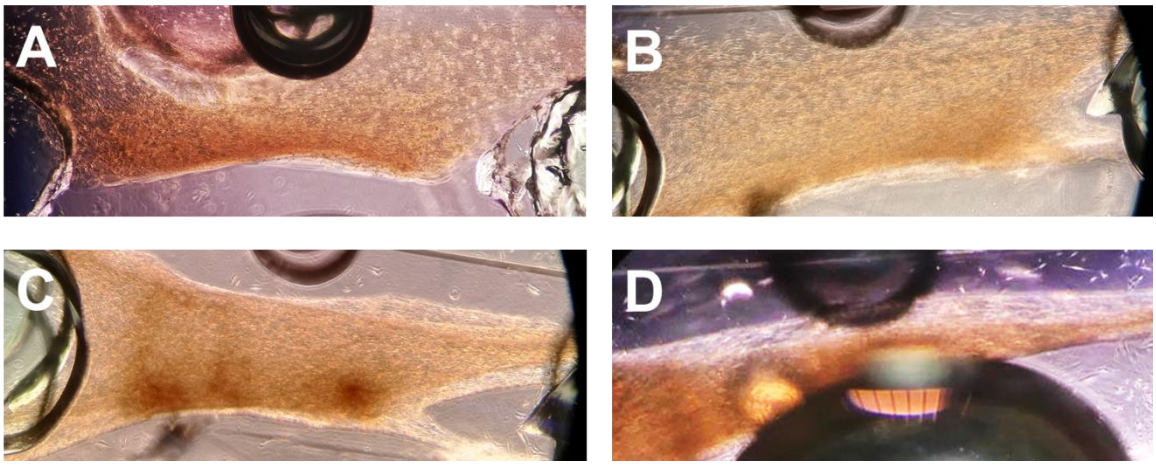

Figure 16: Tendon-like structures. *Microfluidic chip with cigar shaped main chamber loaded with 1200 equine tenocytes in a collagen hydrogel (4 mg/mL)* ***(A)*** *slight condensation of the collagen hydrogel after 2 days* ***(B)*** *cells starting to align after 4 days* ***(C)*** *tendon-like structure after 7 days* ***(D)*** *construct starts to collapse after 10 days*

After four days, the tenocytes seemed to align along the longitudinal axis of the gel. One gel showed a condensed tendon-like shape and was anchored between the pins after 7 days. On day 10, the structure started to collapse and ruptured on day 11. For most of the hydrogels, migration of cells from the gel to the chamber surface was observed.

3.3 Pilot experiment 2 – collagen concentration

Hydrogel drops of three different collagen concentrations were pipetted on a 24-well-plate. The plate was examined after 24 hours, after 3 days and after 7 days of incubation. The addition of medium after either 90 or 120 minutes did not affect collagen polymerization or stability. For the drops of the lowest collagen concentration (2.2 mg/mL), boundaries were hardly detectable under the light microscope (see fig. 17). For a concentration of 3.3 mg/mL collagen, the edges of the drops were more clearly visible and in case for 4 mg/mL the edges were very distinct.

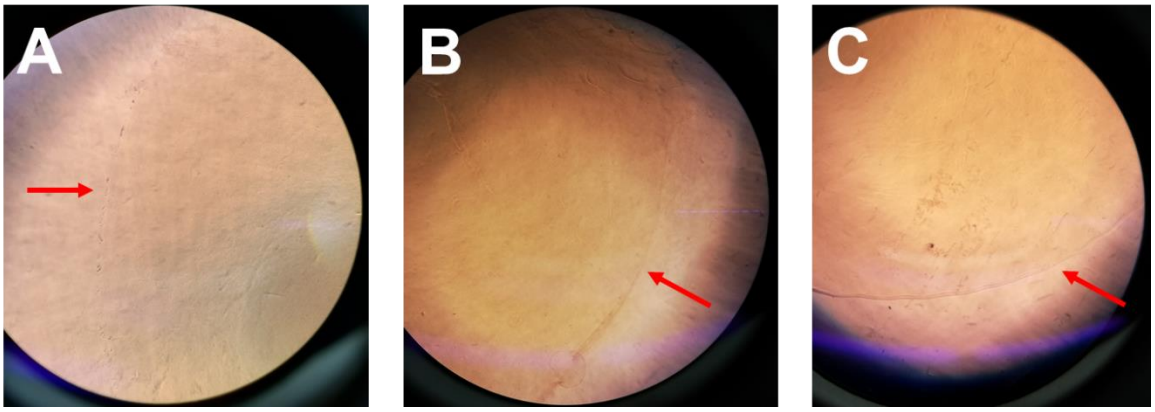

Figure 17: Collagen drops. ***(A)*** *2.2 mg/mL collagen: boundary of the drop is very unclear* ***(B)*** *3.33 mg/mL collagen: boundary more clearly visible* ***(C)*** *4 mg/mL collagen: boundaries are very clear*

3.4 Pilot experiment 3 – tendon on a chip

Microfluidic systems loaded with 80000 equine tenocytes formed tendon-like structures within 4 to 7 days (see fig. 18: A). These condensed further until day 14. For biochips containing 1200 or 30000 cells, no tendon-like structures could be achieved after 14 days (fig. 18: B, C).

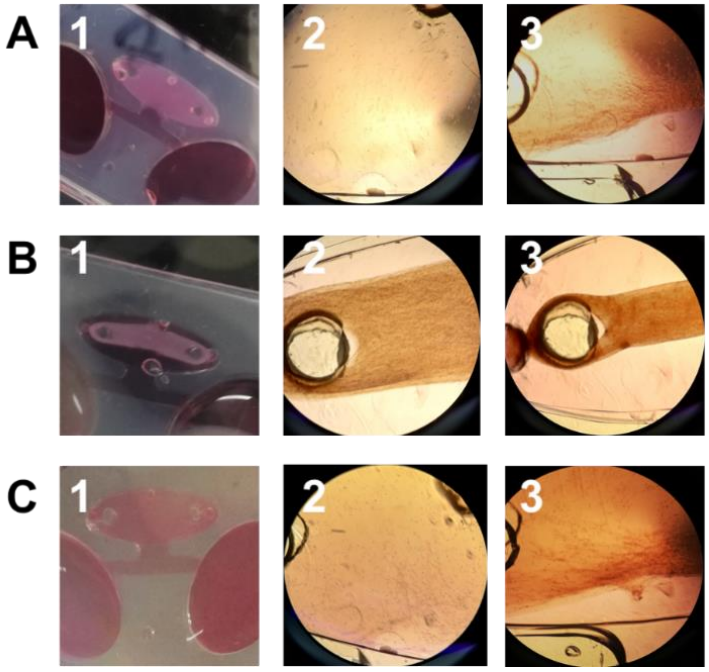

Figure 18: Tendon-on-a-chip. *1 = day 4 macroscopic picture, 2 = day 4 light microscope 4x,3 = day 14 light microscope 4x* ***A)*** *4 mg/mL collagen loaded with 1200 tenocytes* ***(B)*** *4 mg/mL collagen loaded with 80000 tenocytes* ***(C)*** *4 mg/mL collagen loaded with 30000 tenocytes*

The hydrogel of non-tendon-forming chips showed slight condensation in the area where the main chamber meets the medium channel. Cells appeared to accumulate there after approximately 7 days.

3.4.1 MTT assay

After 1 hour of incubation, the tendon-like construct displayed a clear change of color, indicating presence of living cells (fig. 19).

Figure 19: Cell survival on the chip – MTT assay. *4 mg/mL collagen hydrogel loaded with 80000 equine tenocytes.*

3.4.2 FDA/PI Assay

Pictures were taken after 14 days of cultivation with EVOS FL Auto at the pin area. Filters used were Texas Red (fig. 20: A) and GFP (fig. 20: B) to visualize cell survival in the microfluidic chip. Living and dead cells were detected.

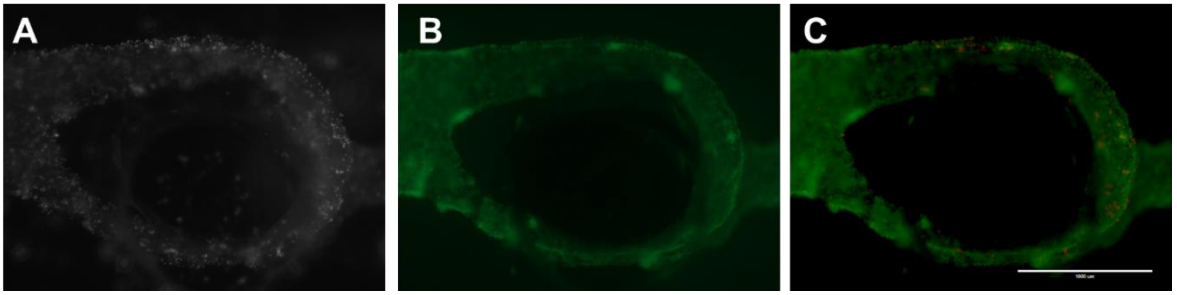

Figure 20: Cell survival on the chip – FDA/PI assay. *4 mg/mL collagen hydrogel loaded with 80000 equine tenocytes. Picture taken at the area of the pin after 14 days. Fluorescence overlay pictures taken with EVOS FL Auto using GFP and Texas Red filter* ***A)*** *Texas Red filter* ***(B)*** *GFP filter* ***(C)*** *Fluorescence overlay picture (GFP and Texas Red)*

3.4.3 Histology

The tendon-like structure was harvested from the microfluidic system after 14 days of cultivation and was subjected to an MTT assay prior to harvest. In the histological section (hematoxylin and eosin (HE) staining) the cells in the organoid appear not elongated, but roundish or cigar-shaped (fig. 21). The tenocytes formed clusters and were not homogenously distributed in the tissue. Histologic processing (embedding in paraffin, tissue section and the HE staining) was carried out by the institute of Embryology and Histology at the Department of Pathology at the University of Veterinary Medicine Vienna.

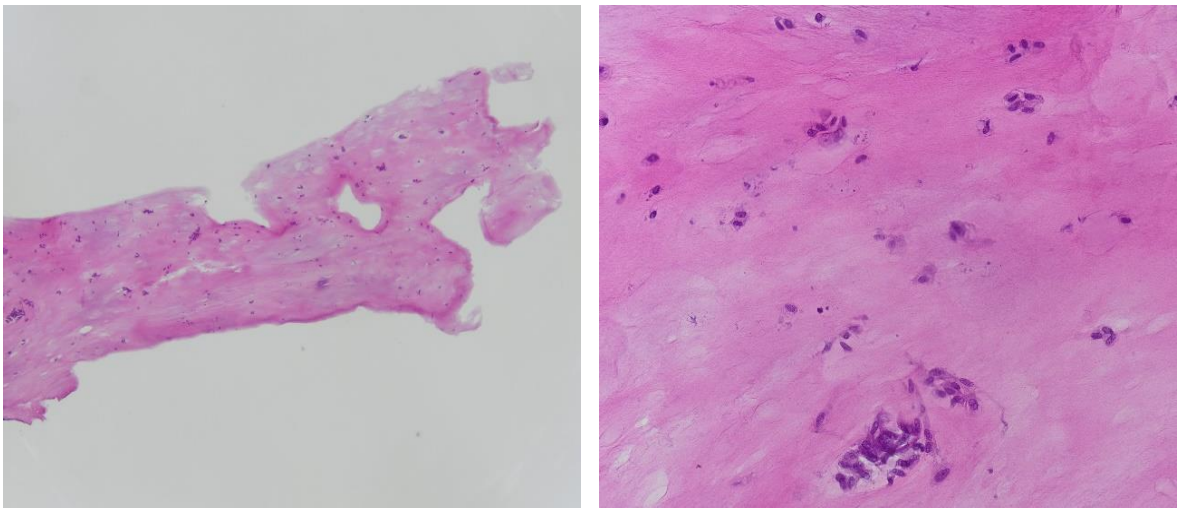

Figure 21: Histological section of the tendon organoid. *Hematoxylin and eosin (HE) staining after 14 days of cultivation: tissue appears pinkish, cells are stained purple*

3.5 Pilot experiment 4 – hydrogel rigidity & permeability

The hydrogel rigidity was measured in triplicates for each collagen concentration (2.2 mg/mL, 3.33 mg/mL and 4 mg/mL) in mmHg using a tonometer. The mmHg values were converted to kPa by multiplication with the factor 0.133322. The mean rigidity is presented in the table below (tab. 5):

Table 5: Mean rigidity in mmHg and kPa *for 2.2 mg/mL, 3.33 mg/mL collagen and 4 mg/mL collagen with sample size and relative standard deviation*

		Rigidity		
Collagen concentration	sample size	mmHg	kPa	%RSD
4 mg/mL	n=3	24.4	3.3	20.5
3.33 mg/mL	n=3	15.6	2.1	3.7
2.2 mg/mL	n=3	10.2	1.3	12.6

Significant differences in hydrogel rigidity (fig. 22) were found comparing the three collagen concentrations with an unpaired t-test: the 3.33 mg/mL collagen hydrogel was significantly more rigid than the 2.2 mg/mL gel ($p = 0.0116$). With 3.3 kPa or 24.4 mmHg the highest collagen concentration (4 mg/mL) was the most rigid with significant difference to 3.33 mg/mL ($p = 0.0085$) or 2.2 mg/mL ($p = 0.0027$).

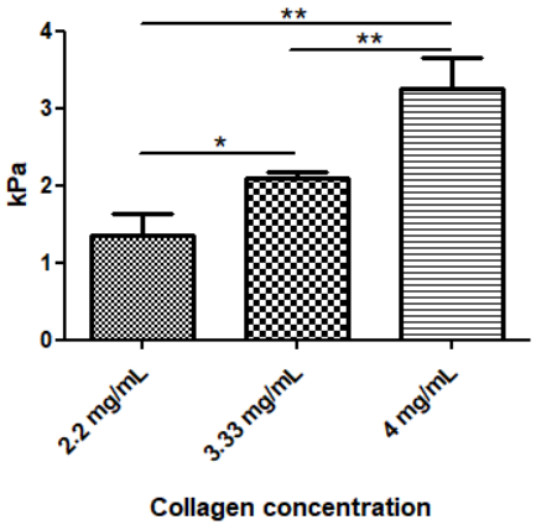

Figure 22: Hydrogel rigidity *in kPa for 2.2 mg/mL, 3.33 mg/mL and 4 mg/mL collagen hydrogels. Significance levels are shown as "*" for $p < 0.05$ and "**" for $p < 0.01$*

To evaluate whether increasing hydrogel rigidity correlates to increasing collagen concentration, a linear model was fitted to the rigidity curve plotting the elastic modulus (kPa) against the collagen concentration (fig. 23). The r-squared value was 0.8518.

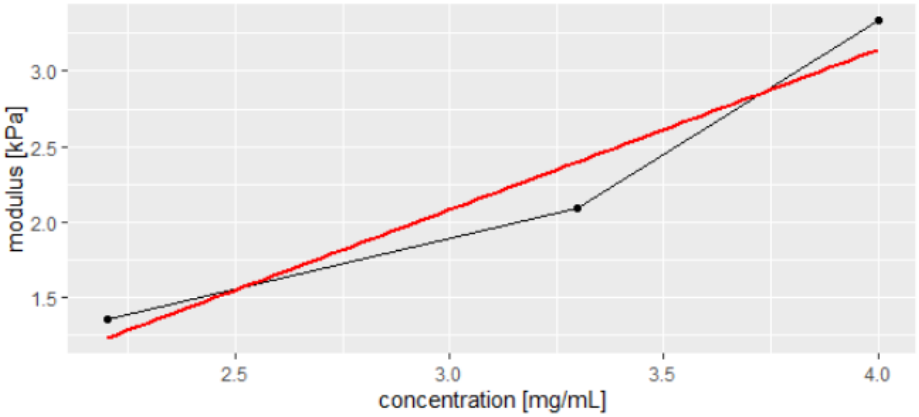

Figure 23: Linear model of hydrogel rigidity *in kPa plotted against the collagen concentration. R-squared = 0.8518*

To assess the hydrogel permeability of 2.2 mg/mL, 3.33 mg/mL and 4 mg/mL collagen hydrogels, the diffusion of fluorescein into the hydrogel was determined on-the-chip. The diffusion coefficient is plotted in fig. 24. A significant difference in permeability was found comparing the 2.2 mg/mL and the 4 mg/mL collagen hydrogel ($p = 0.0321$). The mean diffusion coefficient was 5.82 µm/min for 2.2 mg/mL collagen, 4.31 µm/min for 3.33 mg/mL collagen and 2.94 µm/min for 4 mg/mL collagen.

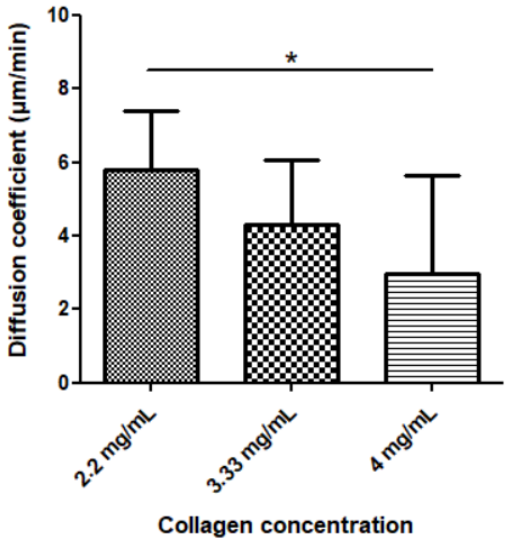

Figure 24: Diffusion coefficient *in µm per minute for 2.2 mg/mL, 3.33 mg/mL and 4 mg/mL collagen hydrogels on-a-chip. Significance level shown as "*" for $p < 0.05$*

3.6 Pilot experiment 5 – cell condensation and survival

Cell-containing drops of two different collagen concentrations were pipetted on a 24-well-plate and the size of each drop was marked to track the initial drop size. During 14 days of cultivation, the diameter of the hydrogel drops did not vary for either concentration (3.33 mg/mL, 4 mg/mL and 5 mg/mL) of collagen (compare fig. 25: A1 - C1).

For all cell-containing collagen drops (3.33 mg/mL and 4 mg/mL), the height of the drops decreased considerable, turning the drop into a disc-like structure (see fig. 25: A2, B2). The 5 mg/mL collagen drops, that contained no cells, did not flatten. After approximately 5 days of cultivation, some cells emigrated from the hydrogel to the bottom of the dish.

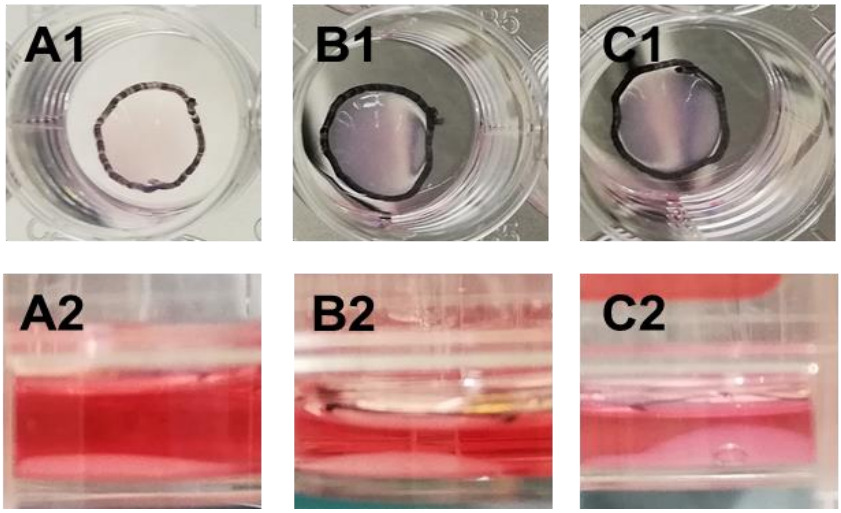

Figure 25: Condensation of the collagen hydrogel. *Perspective: 1 = dorsal, 2 = lateral* ***(A)*** *3.33 mg/mL collagen loaded with 1200 tenocytes* ***(B)*** *4 mg/mL collagen loaded with 1200 tenocytes* ***(C)*** *5 mg/mL pure collagen*

3.6.1 MTT assay

On day 14, the presence of living cells was examined using a MTT assay. For all cell containing collagen constructs, a distinct change of color was observed (see fig. 26: A/B). The control group showed no color shift and did not indicate any metabolic activity (fig. 26: C).

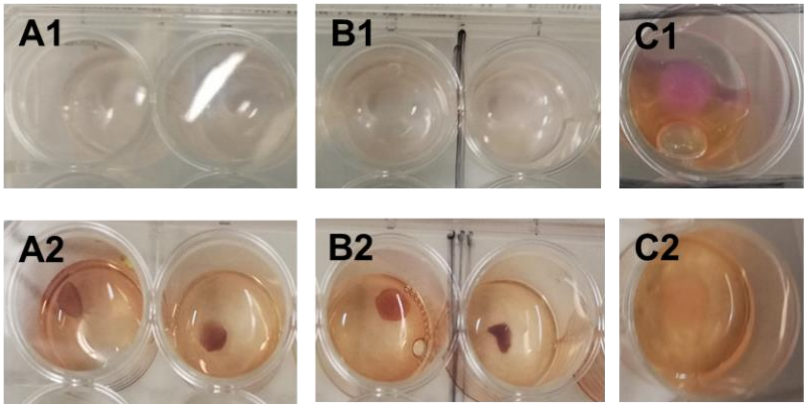

Figure 26: Cell survival in Collagen – MTT assay. *Top row (1) = before incubation, bottom row (2) = after 1 hour incubation* ***(A)*** *3.33 mg/mL collagen loaded with 1200 tenocytes* ***(B)*** *4 mg/mL collagen loaded with 1200 tenocytes* ***(C)*** *control group with 5 mg/mL pure collagen*

3.6.2 FDA/PI Assay

The collagen constructs were stained with FDA and PI to make live and dead cells visible after 14 days of incubation. Pictures were taken with EVOS FL Auto using GFP and Texas Red filters. 3.33 mg/mL and 4 mg/mL collagen constructs showed green fluorescent FDA stained (living) cells (see fig. 27: A/B). For the control group (5 mg/mL) neither green nor red fluorescent cells could be detected (fig. 27: C). No construct showed PI signal (red fluorescence) after one hour of incubation. The samples were reevaluated after an additional incubation period of one hour and some red fluorescent cells were detected.

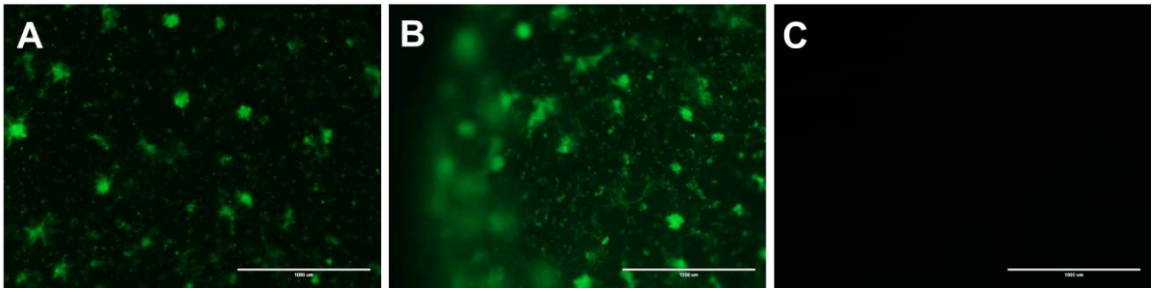

Figure 27: Cell survival in Collagen – FDA/PI assay. *Fluorescence overlay pictures taken with EVOS FL Auto using GFP and Texas Red filter* ***A)*** *3.33 mg/mL collagen loaded with 1200 tenocytes* ***(B)*** *4 mg/mL collagen loaded with 1200 tenocytes* ***(C)*** *control group with 5 mg/mL pure collagen*

3.7 Pilot experiment 6 – tendon defect

Biochips seeded with 80 000 tenocytes in a 4 mg/mL collagen hydrogel were mechanically injured once or twice using a biopsy punch after 14 days of cultivation. Both tendons showed a very distinct macroscopic appearance after 4 weeks of cultivation. The chip with two mechanical injuries appeared weak and close to rupture (fig. 28: B) 14 days after introducing the injuries, while the chip with only one injury appeared to be in a better condition (fig. 28: A).

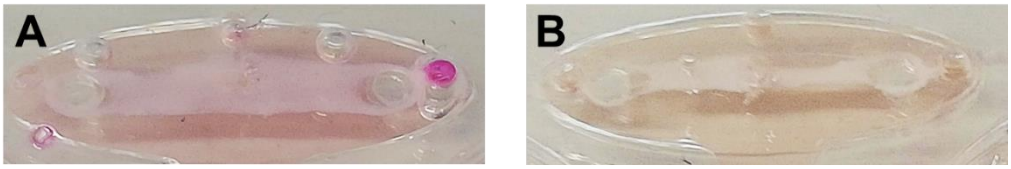

Figure 28: Mechanical tendon injury. *4 mg/mL collagen hydrogel loaded with 80000 equine tenocytes. Pictures taken after 28 days of cultivation, 14 days after injury.* ***A)*** *one-time injured organoid* ***(B)*** *two-times injured organoid*

3.7.1 FDA/PI Assay

Both tendons contained living cells after a total cultivation period of 28 days with 14 days of injury. The scan picture of the entire tendon-like structure using phase contrast, shows the weak appearance of the tendon with two injuries (fig. 29: B1) compared to that with only one injury (fig. 29: A1). Both tendons showed evenly distributed signals of living (green) and dead (white) cells. The sites of injury did not exhibit a greater amount of dead cells.

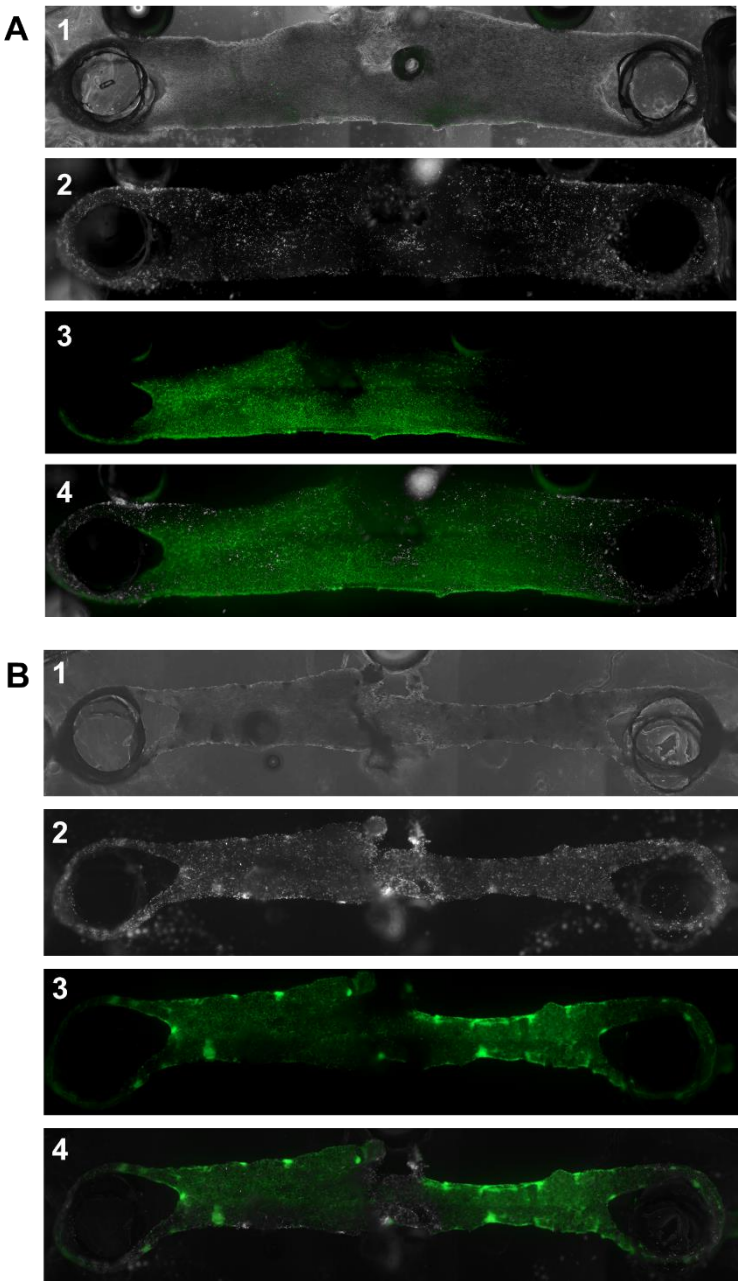

Figure 29: Mechanical tendon injury – FDA/PI assay. *4 mg/mL collagen hydrogel loaded with 80000 equine tenocytes. Scan pictures of the entire tendon-like structure taken with EVOS FL Auto using (1) phase (2) Texas Red and (3) GFP filter. (4) Fluorescence overlay picture of Texas Red and GFP filter* ***(A)*** *tendon with one injury* ***(B)*** *tendon with two injuries*

3.8 Preliminary experiment 7 – “pin variation”

To evaluate whether continuous or non-continuous PDMS pins are more suitable for the mechanic stimulation of tendons-on-a-chip, three variations of pin designs were tested. Tendon-like structures have been formed on all chips, regardless of the pin design. Upon mechanical stimulation using the LEGO® device, chips with pins of the non-continuous and semi-continuous design failed to transmit the strain to the tendon-like structure. After a few stretches, the tendon would slip over the tip of the pin (fig. 30). The continuous design, where both pins are connected to the ceiling of the main chamber, was the only one to reliably exert strain.

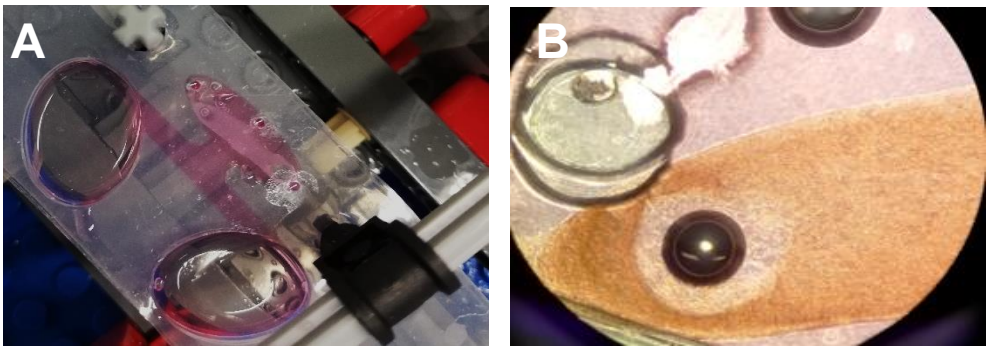

Figure 30: Semi-continuous pin design. *The tendon-like structure slipped over the end of the pin after being stretched* ***(A)*** *macroscopic* ***(B)*** *microscopic picture*

3.9 Preliminary experiment 8 – characterization of tendon strain

Biochips with 80 000 tenocytes in a 4 mg/mL collagen hydrogel and 0.5 % fluorescent beads were loaded to determine the deflection of single cells in the tendon organoid. Tendon-like structures were observed for all chips after 5 days of cultivation. Chips which had a glass slide attached, failed to be stretched by the LEGO® device. For the characterization of strain conducted to the tendon, only chips without glass slides were investigated. Tendon-like structures did not rupture upon stretching.

The applied strain was calculated for 5 different microfluidic chips. For three different positions (origin, center, termination) on each chip, the deflection of single green fluorescent particles in the tendon-like structure was quantified (fig. 31) and the average was calculated.

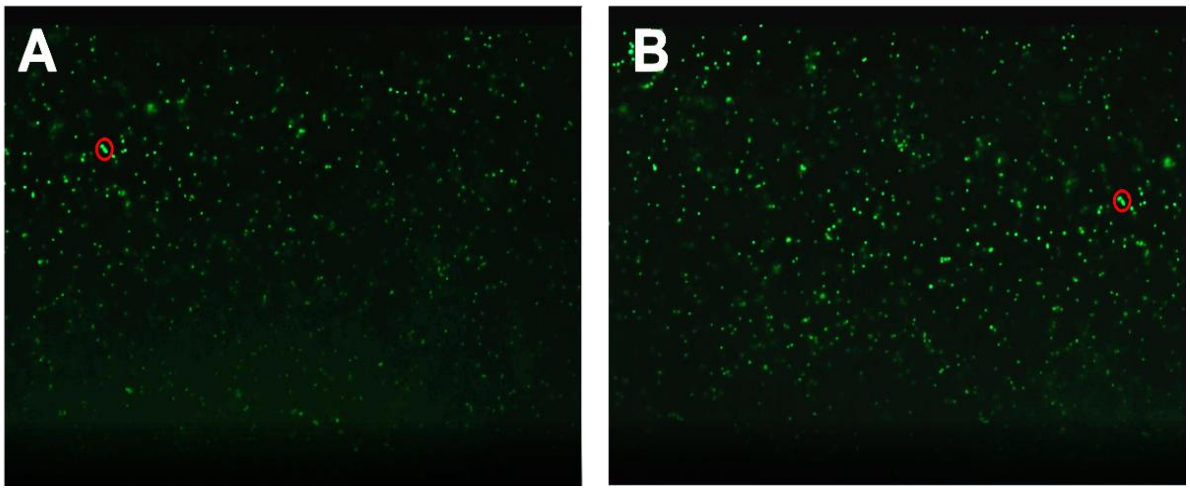

Figure 31: Deflection of green fluorescent particles. *4 mg/mL collagen hydrogel loaded with 80000 equine tenocytes and 0.5 % green fluorescent polymer microspheres. Fluorescence pictures taken with EVOS FL Auto using GFP filter. The red circle marks the particle position in* ***A)*** *unstrained and* ***(B)*** *strained state.*

At the three measurement areas (origin, center, and tail), similar values of strain were detected for all biochips (fig. 32: A). Strain variation for all chips did not exceed 1.9 % at any region of the tendon-like structure. However, comparing the three measurement regions, strains differed significantly. For the origin, which is the least strained area of the tendon-like structure, values of 9.9 to 11.8 % of strain were recorded (fig. 32: B).

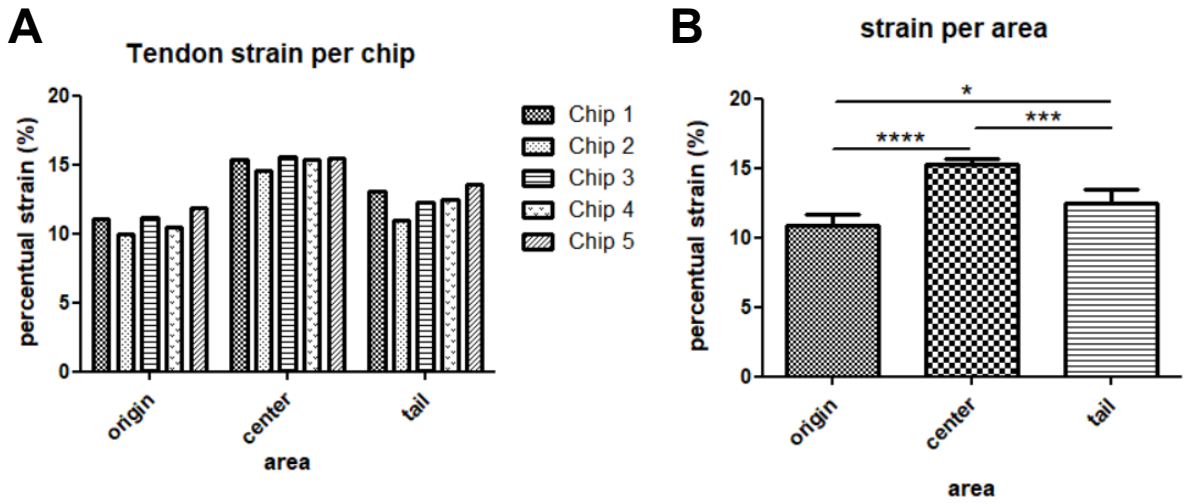

Figure 32: Characterization of tendon strain. A) *Percentual tendon strain per chip (1-5) plotted for each area* ***(B)*** *Average of tendon strain per area. Significance levels are shown as "*" for p < 0.05, "***" for p < 0.001 and "****" for p < 0.0001*

The center of the organoid is the most-strained region and showed a percentual strain of 14.5 to 15.5, which differs significantly from the origin ($p < 0.0001$) and the tail ($p = 0.0004$). In the tail area, strains of 10.9 to 13.6 % were recorded. These strain values are significantly higher than those of the origin ($p = 0.022$).

3.10 Mechanical tendon stimulation on-a-chip

To evaluate the influence of mechanical training on tendons-on-a-chip, biochips loaded with 80 000 tenocytes in a 4 mg/mL collagen hydrogel were daily subjected to cyclic uniaxial strain using a Lego® device (fig. 33). The microfluidic PDMS chips as well as the tendon-like organoids withstand two weeks of daily mechanical loading using the LEGO® device. None of the tendon-like structures ruptured.

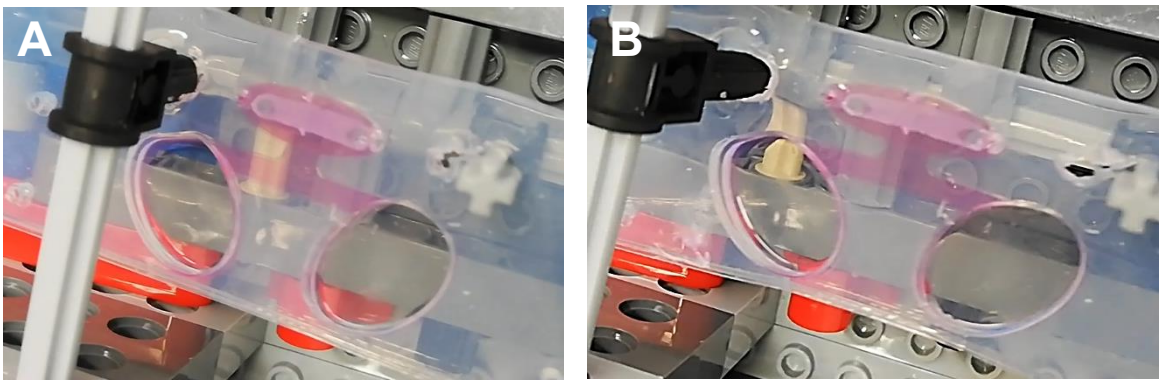

Figure 33: Mechanical tendon straining *using the Lego® construct.* ***(A)*** *unstrained organoid* ***(B)*** *strained organoid*

3.10.1 qPCR

Samples were harvested after 14 days of mechanical loading and RNA was isolated as described in 2.5.1. RNA yield for all samples were not measurable using the Nanodrop and were therefore re-measured using Qubit. Again, for all samples the RNA value was “too low” to be quantified. Therefore, it was decided to pool all biological and technical replicates of the same groups. The RNA was reprecipitated, washed and diluted in nuclease-free water. Using the Qubit RNA HS assay kit, an RNA content of 5.52 ng/µl was determined for the mechanically stimulated samples that were pooled. For the control

group, the RNA content remained too low to be quantified. A qPCR reaction was carried out but failed.

3.11 Tendon inflammation

To examine the influence of inflammatory mediators and/or mechanical injuries on the tendon-like structure, tendons-on-a-chip were divided into 4 groups: healthy, healthy with injury, inflamed and inflamed with injury. Organoids of the group “healthy” did not show any remarkable changes in their gross appearance within the culture period (see fig. 34). The “healthy injured” group showed only marginal optical changes. For all samples that were treated with inflammatory medium, distinct alterations of appearance were found after 7 and 14 days of treatment. The organoid got thinner with time and appeared very fragile, especially in the area of the pins.

Further it was to be observed that with ongoing culture period, the edges of all inflamed organoids appeared more and more uneven when compared to healthy tendon-like structures (fig. 34: A1 to A3 and B1 to B3).

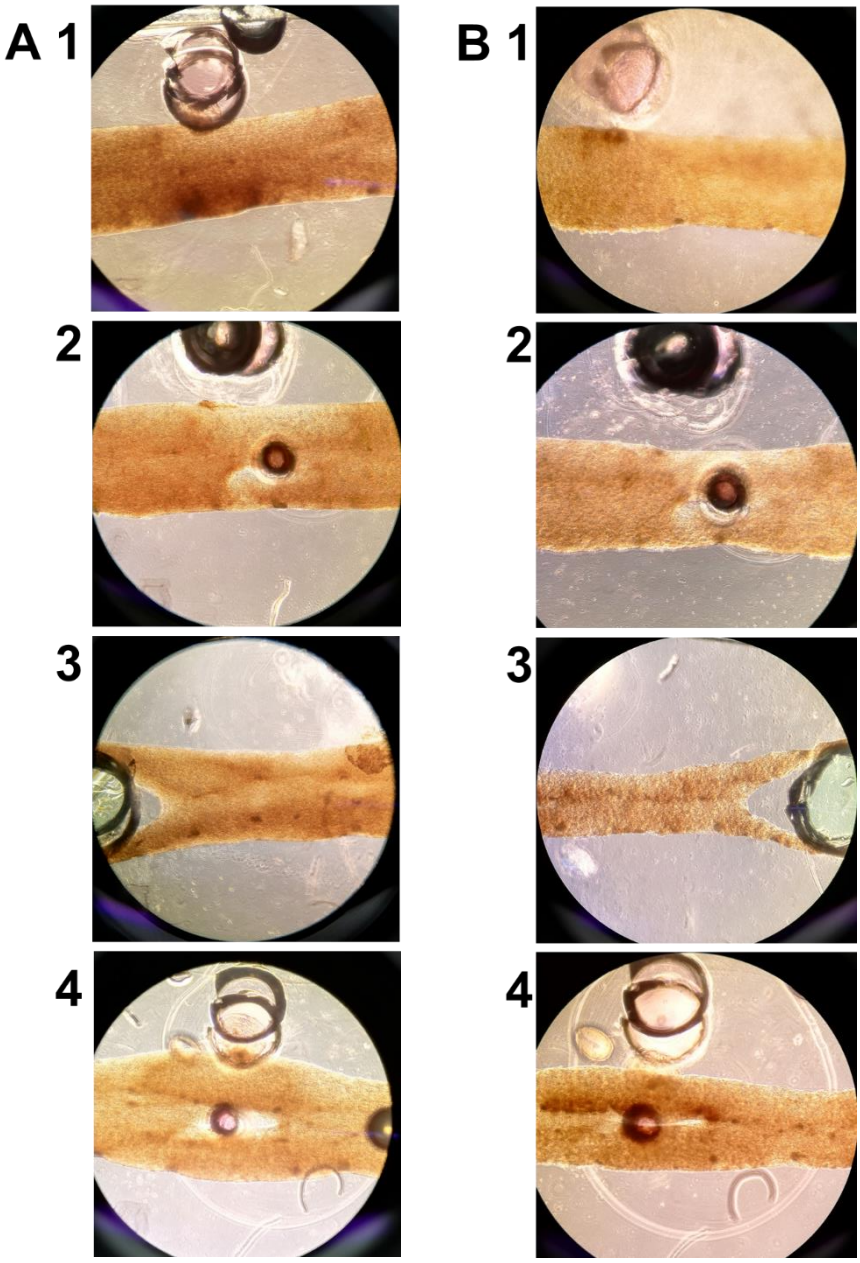

Figure 34: Tendon inflammation *of Donor 1. Pictures taken with the light microscope at 4x magnification after* ***(A)*** *7 days and* ***(B)*** *14 days of treatment:* ***(1)*** *healthy* ***(2)*** *healthy injured* ***(3)*** *inflamed* ***(4)*** *inflamed injured.*

The lesions of all samples that were mechanically injured, stayed almost unchanged (fig. 35). No signs of “healing” of the injury could be observed in either group, although the overall organoid condensed further and therefore the edges of the lesion appear closer together (fig. 34: A4, B4).

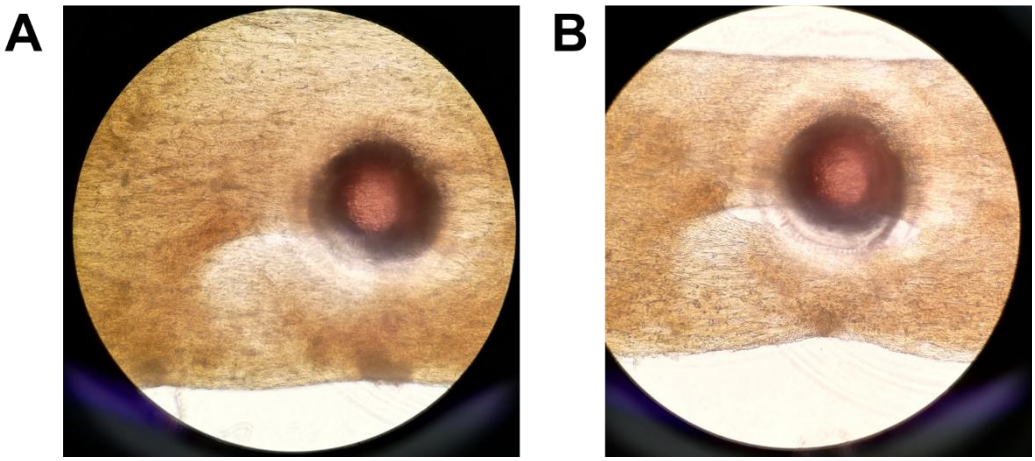

Figure 35: Tendon injury. *Light microscope picture with 10x magnification* ***(A)*** *Day 4 after injury* ***(B)*** *Day 14 after injury*

3.11.1 qPCR

All genes tested were normalized to the levels of the house keeping genes. The relative mRNA levels of Col1a2, Mkx and MMP13 are presented below (fig. 36). For Col1a2 no significant differences between a culture duration of 7 and 14 days were observed ($p > 0.05$), except for the inflamed injured group where Col1a2 expression was distinctly lowered after 14 days ($p = 0.0055$). A significant increase in Mohawk gene expression was observed for inflamed samples after 14 days when compared to 7 days ($p = 0.0147$).
In case of MMP13, again, the only significant difference between 7 and 14 days of culturing was observed for the inflamed group ($p = 0.0312$).

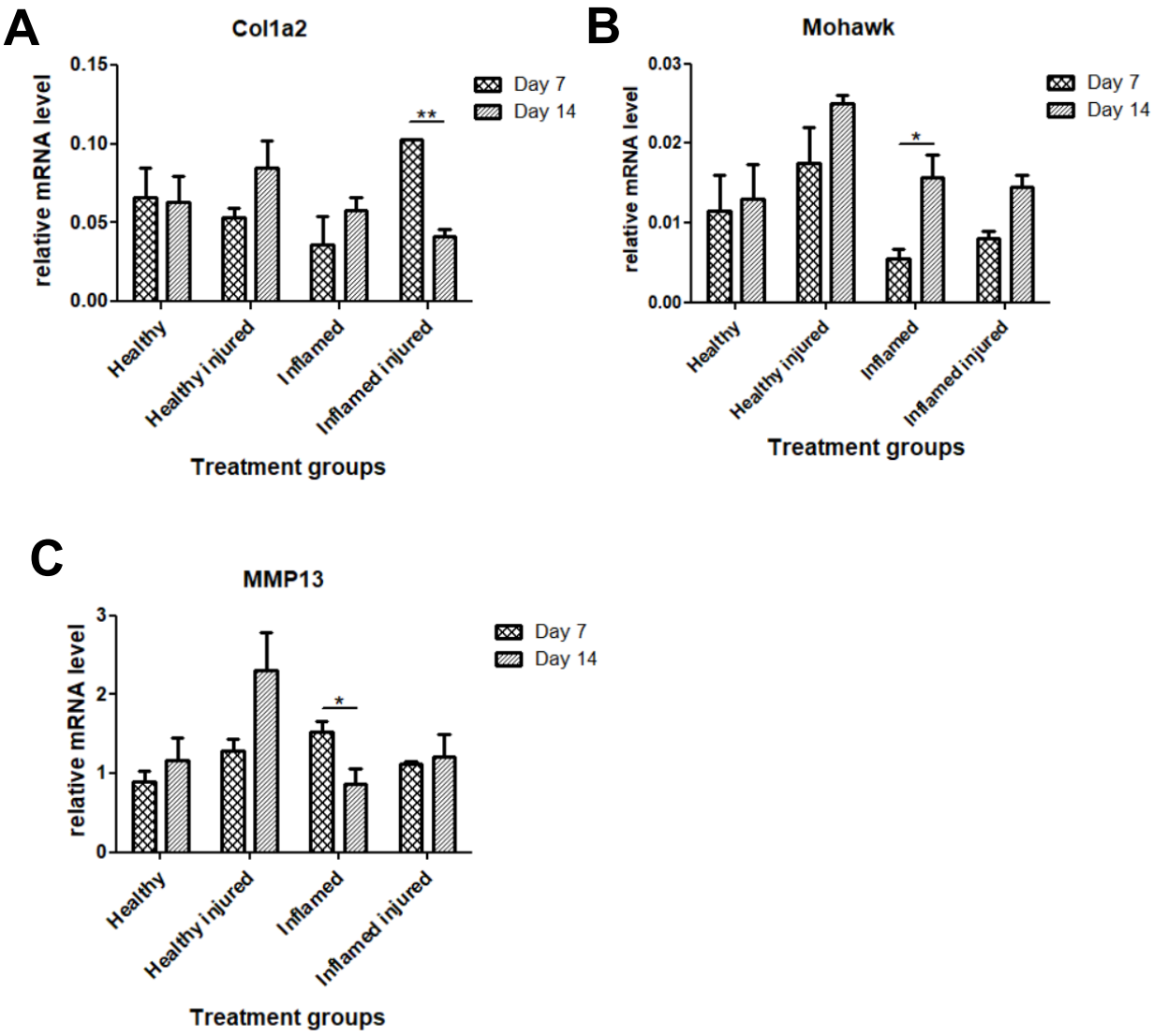

Figure 36: qPCR comparing tendon inflammation after 7 and 14 days A) *relative mRNA levels of Col1a2,* ***(B)*** *relative mRNA levels of Mohawk, and* ***(C)*** *relative mRNA levels of MMP13 for each treatment group (healthy, healthy injured, inflamed, inflamed injured). Significance levels are shown as "*" for p < 0.05 and "**" for p < 0.01*

For Donor 2 and Donor 3, samples were harvested after 14 days of treatment and the RNA was isolated as described in 2.5.1 RNA isolation and concentration. Due to a very low RNA yield, all samples were re-measured using Qubit. Except for 7 samples, the RNA values were "too low" to be quantified. For these 7 samples, RNA levels were 4 to 9 ng/µL. Therefore, it was decided to pool all biological and technical replicates of the same groups. The RNA was reprecipitated, washed and diluted in nuclease-free water. For each pooled

group (healthy, healthy injured, inflamed, and inflamed injured), the RNA content was measured again with Qubit RNA HS assay kit. RNA values measured were 6.22 to 21 ng/µl. The qPCR was performed as described in 2.5.3 quantitative PCR. Gene levels were normalized, and the relative mRNA level is plotted below (fig. 37).

The level of gene expression for all tenocyte markers (Col1a2, Mkx and Scx) did not show any significant changes comparing the different groups (fig. 37: A, B, C). For MMP13 (fig. 37: D), no significant differences were reported comparing the groups except for healthy to inflamed injured tendons ($p = 0.0291$). In the case of IL-6 (fig. 37: E), the expression was significantly higher for the inflamed group compared to all other treatments (healthy: $p = 0.0007$; healthy injured: $p = 0.0009$; inflamed injured: $p = 0.0012$). Further, significant differences of mRNA expression were also found comparing the healthy control group to the inflamed injured ($p = 0.0013$) and comparing the healthy injured to the inflamed injured group ($p = 0.0049$).

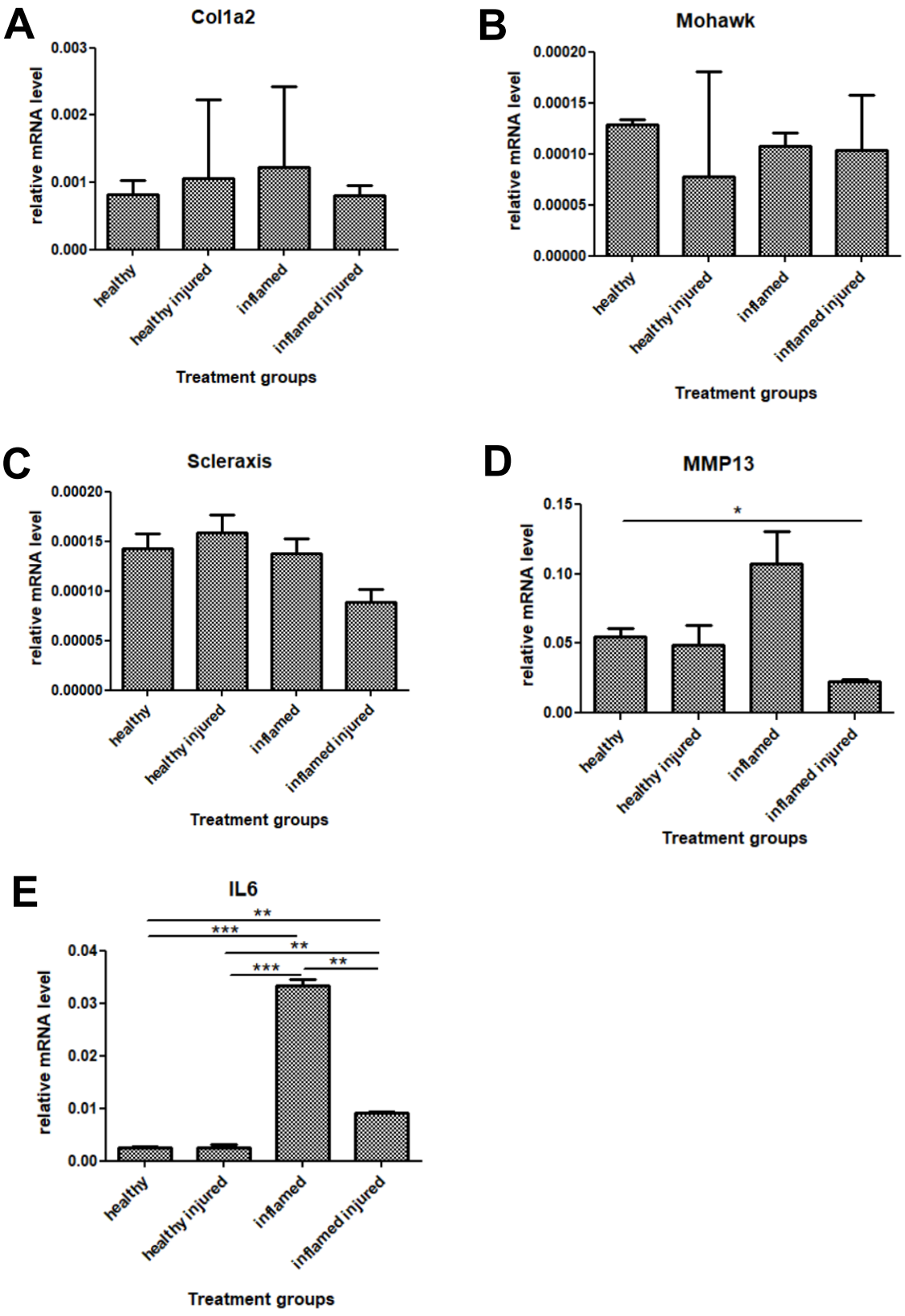

Figure 37: qPCR of tendon treatment after 14 days. *For each group (healthy, healthy injured, inflamed, inflamed injured) the* ***A)*** *relative mRNA levels of Col1a2* ***(B)*** *relative mRNA levels of Mohawk* ***(C)*** *relative mRNA levels of Scleraxis* ***(D)*** *relative mRNA levels of MMP13* ***(E)*** *relative mRNA levels of IL6 was plotted. Significance levels are shown as "*" for $p < 0.05$, "**" for $p < 0.01$ and "***" for $p < 0.001$*

4. Discussion

The aim of this thesis was to establish an organ-on-a-chip system that allows for the 3D cultivation of tendon organoids. These tendon-like structures should further be subjected to biomechanical stimuli and be used as a future disease model. To enable a three-dimensional cultivation of primary equine tenocytes, three different biochip designs and variations of pins were created and tested. All designs are based on the size of a standard glass slide (26 x 76 mm). It was decided to use the oval chip design with continuous pins of 1.5 mm diameter for further experiments, as it enables proper loading of the main chamber without massive air inclusions or bubble formation and allows for mechanical loading of the mini tendon. A Lego® construct, operated by two (initially only one) Lego® engine, was built to carry out a cyclic stretching movement, but failed to stretch the biochip long-term.

The strain the Lego® device conducts to the mini tendon on-the-chip was determined using fluorescent beads. The chip-to-chip variation of strain did not exceed 1.9 %. In the literature, strains of approximately 8 % and exceeding are reported to induce macroscopic failure and possibly trigger tendon rupture[3,18]. The origin, which is the least strained area of the tendon-on-a-chip, was exposed to strains of 9.9 to 11.8 %. For the tendon tail, corresponding but slightly higher strain values of 10.9 to 13.6 % were detected. The center of the tendon is the most strained region, for which strains of up to 15.5 % were achieved without rupture. The tendon-on-a-chip model presented in this study represents a pathophysiologic strain model. Nevertheless, with adjusted settings the presented system could also exert biomechanical stimuli in the physiological range. It was reported that the equine SDFT experiences strains of approximately 2.5 % at the walk, 4.15 % at the trot[60] and 11.5 % to up to 16 % at the gallop[3,60]. When carrying a rider, the SDFT is strained even more[60]. In a non-domesticated setting, horses spend up to 16 hours per day walking and grazing. Horses walk at a frequency of 0.97 Hz, trot at 1.59 Hz and gallop at a frequency of 2.01 Hz[61].

It was observed, that the PDMS biochip is distorted when being stretched, which could be one reason for the 1.9 % chip-to-chip bias that was observed. Nevertheless, the biochip itself and the tendons-on-a-chip withstand 15 minutes of daily biomechanical stimulation for at least 14 days without rupturing. It has previously been reported that PDMS can be stretched and returns to its initial shape[62]. To prevent the edges of the chip from excessive bending, some kind of guideway could be introduced to the Lego® construct. The use of a glass slide, attached

in the area of the medium reservoirs for more stability, is not recommended, as it reportedly prohibits any stretching of the chip. Another reason for chip to chip variation may be that their manufacture involves some manual work. Smallest deviations when bonding the individual layers or when placing the pins in the main chamber may result in altered strain. An alternative for biochip production may be replica molding, where liquid PDMS is filled into a negative copy of the desired mold[50,55], thereby creating biochips in a more standardized manner. Still, it was reported that chips manufactured with a master mold are not perfectly uniform as well, displaying differences no worse than 0.05 mm[63]. However, for an entire chip thickness of 1.2 mm[63], the chip-to-chip bias would therefore amount to up to 4.16%.

For loading of the microfluidic chambers, two natural hydrogels were initially considered for the 3D cultivation of tenocytes: fibrin and collagen hydrogel. Fibrin is an essential part of the coagulation cascade and important for wound closure[33,64]. Its precursor, fibrinogen, is cleaved by thrombin, which initiates clotting[33,64]. Due to its biocompatibility, it is widely used in clinical settings[33]. Dependent on the ratio of thrombin to fibrinogen, the hydrogel microstructure differs[33,64]. Increased amounts of thrombin result in thinner fibrils and small pores[33,64].

Collagen hydrogels are an obvious choice as collagen type I, the major component of these hydrogels, is also a major component of tendon ECM[3–5,8,20,25]. Comparable to its native counterpart, collagen hydrogels are polymers of crosslinked fibrils and fibers[33,65]. Moreover it has been shown that the expression of characteristic tendon markers is increased in 3D cultured tenocytes using collagen as matrix[11]. A major drawback of both, collagen and fibrin, is their susceptibility to cell-mediated degradation by cellular proteases and their limited long-term stability[33].

During the preliminary experiments, it was decided to use collagen gel, as the high viscosity of the fibrin gel hampered proper pipetting and chip loading. Moreover, when comparing the two hydrogels, not a single fibrin gel stayed intact on-the-chip. The collagen concentrations used for later experiments were chosen based on drop-stability as major problems were faced when loading the first chips, it was attempted to create a stable drop within the main chamber to avoid floating into the medium channel. Higher concentrations of collagen displayed the best properties for our purposes, hence it was decided to use 3.33 and 4 mg/mL collagen for further experiments evaluating cell survival and gel condensation. This is supported by the findings of Valero *et al.* (2018) that hydrogels of lower collagen content tend to float out of the chamber[65].

The collagen concentration directly influences hydrogel permeability and rigidity[65,66]. For collagen hydrogel permeability it was reported that increasing the collagen concentration decreases the diffusion rate[66]. Again, these findings are in accordance to the results of our experiments which determined gel permeability by the assessment of fluorescein diffusion into the hydrogel, although only a non-significant trend could have been shown.

Further it has been found that matrix stiffness is linked to changes in its permeability[66]. Collagen hydrogels are low in stiffness[33] and belong to the family of soft gels, which have an elastic modulus of around 1 kPa[49,67]. Stiff gels have an elastic modulus of 30 to 100 kPa[49]. For collagen gels, values of 2.7 ± 0.3 kPa have been reported[49,67]. It has been reported that an increase of the collagen concentration results in higher stiffness and more sites for cell adhesion[65,66]. To determine the stiffness of our gels a tonometer was used. Usually, tonometers using the rebound principle are used to determine the intraocular pressure of animals. In horses, intraocular pressures of 21.0 ± 3.14 mmHg were reported with the Tonovet® tonometer[58]. Any value of 7 to 28 mmHg is considered physiological[68], which would correspond to 0.93 to 3.73 kPa. Therefore, the rigidity of soft gels and the equine intraocular pressure is in a comparable range, making the tonometer a suitable measuring device for our purposes. In the present study we found that collagen hydrogels with concentrations of 4 mg/mL show the highest rigidity values with 3.3 kPa. For 3.33 mg/mL, 2.1 kPa and for 2.2 mg/mL 1.3 kPa were measured. Matrix rigidity moreover appears to play a role in cell morphology[67]. Smooth muscle cells display a rounded phenotype when embedded in soft gel and a more flattened polygonal or dendritic shape when cultured on a stiffer matrix[67].

Biochips containing 80000 equine tenocytes embedded in a 4 mg/mL collagen hydrogel were the only ones to form a tendon-like organoid within 7 days and were successfully cultured without rupture and with living cells for up to 28 days. This finding demonstrates that long-term on-a-chip culture for at least one month using collagen hydrogel is feasible. Optical evaluation of these tendons using light microscopy showed a very high cellularity compared to in vivo tendons, why a lower cell number, 30000 tenocytes per tendon, was tested but unsuccessfully. The histological evaluation of the 80000 tenocytes containing organoid however revealed a very low cellularity and suggests to further increase the cell number.

There were major differences when comparing histological sections of the tendon organoid to sections of native equine tendon tissue. Tendons are tissues of low-cellularity[1,2,5,20,21]. Still, the HE staining of the tendon organoid exhibited very few cells. Either the initial number of cells (80000) seeded into the hydrogel was too low or cells are washed out of the hydrogel when changing the culture medium. This could be answered by further experiments using higher numbers of cells. Additionally, histological evaluation should be carried out at earlier time points to evaluate whether medium changes (which occurred two times a week) rinse cells from the hydrogel.

The histologic sections further revealed that tenocytes in the tendon organoid display roundish and cigar shaped nuclei rather than adopting an elongated phenotype orientated along the long axis of the organoid as to be expected. Roundish nuclei may result from unaligned cells or tenocyte abnormality[30]. Cook et al. (2004) reported abnormal tenocyte appearance in cases of tendinosis. Tendinosis is a chronic pathology caused by the accumulation of small tears which results in degeneration[9,28]. Modified or abnormal tenocytes appear enlarged with a rounded nucleus[30]. Cells that are not aligned could result from a lack of biomechanical stimuli, as tenocytes naturally arrange in the direction of static or dynamic strain. Either the system failed to apply enough strain to the construct, or there is too much matrix for the strain to be effectively transmitted to the cells. Still, this is considered unlikely as the collagen hydrogel drastically condensed to form the tendon-like structure. Hydrogels seeded with less (1200 or 30000 equine tenocytes) or no cells did not show a comparable condensation. Some condensed slightly in the area close to the medium channel, while most did not condense at all. These findings indicate that the hydrogel condensation is linked to cellular behavior (cells contracting the gel) rather than shrinkage of the gel, which further implies that strain is conducted to the cells. This is in accordance to data reported for fibroblasts cultivated in collagen type I gels[69]. It was observed that fibroblasts draw collagen fibers in their proximity closer to their cell body, thereby creating regions of dense fibers around themselves[69]. Simultaneously, the overall hydrogel starts to condense[69]. It is also reported that fibroblasts adopt a less elongated phenotype if embedded in larger collagen fibrils[33]. Hydrogel microstructures are largely dependent on the prevailing temperature during the polymerization process[33,65]. A lower temperature leads to the formation of larger fibrils[33].

Cells with cigar shaped nuclei possibly belong to type II tenocytes naturally found in equine tendons[7]. Nevertheless, all cells found in the tendon organoid are arbitrarily distributed, with most of them forming clusters. A possible reason for the abnormal cellular distribution may be

an inhomogeneous density of collagen. Still, this is rather unlikely as the collagen type I hydrogel (PureCol EZ gel solution, Sigma Aldrich) is a ready-to-use mixture. More likely, the cell suspension was not blended into the viscous collagen thoroughly enough before loading the microfluidic chamber. When mixing, attention must be paid to avoid bubble formation and rapid processing is important to keep the hydrogel from premature polymerization, which is induced by increasing temperature[33]. A well mixing and bubble-free alternative to pipetting would be to vortex the mixture, but this could potently harm the cells.

Another aspect may lie in histological processing as hydrogels are treated identically to soft tissues which can lead to major problems[33]. Hydrogels are water-rich and therefore the excessive dehydration and heating steps, used in paraffin embedding by default, may disrupt the structure of the hydrogel[33]. Retrieved from the chip, the tendon-organoid is very fragile, small and thin. As a result of the water withdrawal, the construct may shrink further, deform or fold[33] and it gets increasingly difficult to accomplish a full-length section of the tendon, especially if the organoid was not embedded perfectly straight. To increase the number of sections that can be made per tendon, the organoid can be rotated along its longitudinal axis (fig. 38).

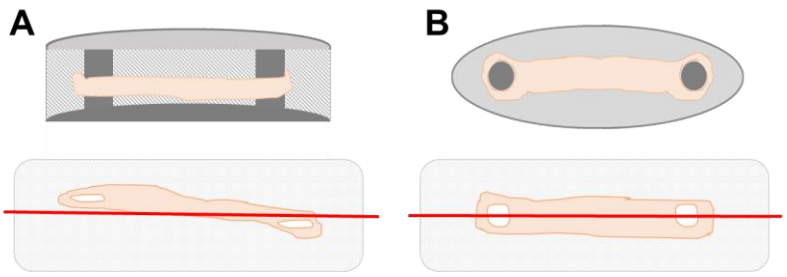

Figure 38: Histologic section *of the tendon-like structure* ***(A)*** *lateral view. Top: on the chip; bottom: embedded in paraffin* ***(B)*** *from above. Top: on the chip; bottom: embedded in paraffin. The red line marks a potential section level.*

Tendinopathy, or more specifically tendinosis, is a chronic pathology resulting from accumulating tears that further lead to tissue degeneration[9,21,28]. As tendons-on-a-chip are meant to serve as future disease models for tendinopathies, the influence of a mechanic injury on-the-chip was examined. Two tendon organoids were prepared and cultured for two weeks before being injured. Post injury and after additional cultivation for 14 days, the tendon that was injured two-times exhibited a more fragile macroscopic appearance than the one that was

injured once. That indicates that two injuries are a greater challenge for the organoid and lead to an instable, close-to-rupture phenotype. Interestingly, the sites of injury or rather the surrounding area did not exhibit increased amounts of dead cells.

Different tendinopathy-like states were compared on-the-chip. The pathology of tendinosis was mimicked by “healthy injured” biochips that were mechanically injured using a biopsy punch. A tendinitis, which describes a pathology of tendon inflammation[9,28], was aimed to be mimicked using culture medium containing the inflammatory factors TNF-α and IL-1β. For the “inflamed injured” group the tendinopathic state induced was a hybridization of tendinosis and tendinitis by combining the use of inflammatory medium with a mechanical injury. At the mRNA level, two markers for tenocytes (Mohawk, Col1a2) and one for inflammation (MMP13) was examined. MMP13 was chosen as it is known to be upregulated in the equine SDFT suffering from tendinitis[70]. For Col1a2 no significant differences between a culture duration of 7 and 14 days were observed, except for the inflamed injured group where Col1a2 expression was distinctly lowered after 14 days. When comparing the mRNA levels of the different groups after 7 days, a trend of decreasing Col1a2 expression linked to injury or inflammation may be observed. This could possibly be explained by the downregulation of collagen type I production due to a switch to collagen type III, which is usually observed when a healing response is mounted[8,21]. Later in this process, the native tendon switches back to collagen type I[8,21]a, which could potentially explain the reelevated levels after 14 days. However, to verify this collagen type III levels must be measured as well.

For Mohawk a distinct increase in gene expression was observed for inflamed samples after 14 days compared to 7 days. Generally, a (non-significant) trend to increasing mRNA levels linked to cultivation time can be observed for all treatment groups except for the control group. This trend is even less prominent for Col1a2 but can be observed for healthy injured and inflamed samples. Such a trend could possibly be explained by cellular activation due to tendon injury or inflammation. This is supported by the findings that tenocytes are activated in tendinopathic tissue[30].

In case of the inflammation marker, MMP13, the only significant difference between 7 and 14 days of treatment was observed for the inflamed group. However, as only two tendons were evaluated per treatment group, the amount of RNA used was very low and the data is hence very susceptible to bias.

Subsequent qPCRs returned melting curves and amplification plots similar to those of the negative controls for all samples and genes tested. As methodological problems such as faulty primer designs or a contamination of the qPCR reagents were excluded by quality control steps including positive and negative controls, we concluded insufficient cell numbers to be the likely cause. One organoid, with an initial amount of 80 000 cells, is a rather low starting value of theoretically retrievable RNA. As RNA is highly instable, any problem during RNA isolation and/ or DNase treatment may have resulted in the poor RNA yields. It was reported that RNA extraction using TRIzol® is suitable for human MSCs embedded in a collagen type I matrix (4 mg/mL)[71]. Still, it should be considered that, in contrast to cetyltrimethylammonium bromide (CTAB) which is a cationic surfactant, the use of isopropyl alcohol does not lead to isolation of mRNA only[71]. Rather, a variety of low-molecular-weight RNAs, like rRNA and tRNA for example, is isolated as well[71]. Therefore, mRNA values may not correspond to the total RNA amount measured and might be lower. Further, it should be noticed that the human MSC samples were pulverized using a BioPulverizer prior to RNA extraction using TRIzol®[71]. In general, either mechanic or enzymatic disruption is used to release cells from tissue constructs[33]. Caution must be paid not to disrupt the integrity of intracellular components[33]. In our case, RNA was retrieved from the organoid by mechanic disruption. Vortexing for 5 minutes could be considered either insufficient to isolate the cells from the collagen matrix or too invasive, leading to impaired RNA integrity and fragmentation.

To increase the RNA amount per treatment group, it was decided to pool all technical and biological replicates. The RNA was reprecipitated, but RNA counts remained rather low. This might be due to an error during RNA isolation or processing as mentioned before but may also result from the sample processing itself. The mechanical stimulation occurred at room temperature, which might have had a negative impact on cell viability. The inclusion of a buffer, for example culture medium with HEPES, during that time was not feasible as medium had to be removed from the chip to avoid spilling.

Samples of the inflammation experiment were pooled and a qPCR was carried out for three tenocyte markers (Col1a2, Mohawk and Scleraxis) and two inflammation markers (MMP13 and IL-6). IL-6 was chosen as a representative marker, as it is known to be upregulated in the painful and pathologic human AT[72]. The relative mRNA levels of the tenocyte markers did not display any significant changes comparing the different groups. For some samples of Col1a2 and Mkx a rather high standard deviation was found within the groups. This could be due to two major reasons: the RNA sample was not mixed well, or a pipetting error occurred. In this

case, a pipetting error is rather unlikely as the PCR was prepared by a robot and the pipetting scheme was checked twice. As the samples of all donors were pooled, an interindividual influence can be excluded.

For the inflammation markers, the relative mRNA levels of the inflamed samples were elevated compared to the other groups, indicating that an inflammatory response was triggered. Nevertheless, for MMP13 only a non-significant trend was found. In the case of IL-6, almost no response could be observed in samples cultured with normal culture medium (healthy and healthy injured). For samples cultured with inflammation medium, distinctly lower IL-6 levels were observed for the injured group compared to the inflamed samples. This difference might result from a downregulation following doubled activation which may have led to overstimulation. As indicated by the significantly elevated IL-6 expression of the inflamed sample, an inflammatory response is triggered by the inflammatory mediators in the medium. A second activator might be mechanical injury, but this is contradicted by the fact that the IL-6 levels of the healthy injured group are similar to the control.

As mentioned before, to accurately measure the behavior of the tendon organoid in response to the presented triggers based on relative mRNA expression, the sample number should be considerably increased to achieve more reliable results in future experiments. Further, to monitor the onset and progression of the inflammatory response, more timepoints should be taken into account and as a next step, biomechanical stimulation should be implemented additionally to each group to mimic the natural tendon environment more closely.

There are already many organ-on-a-chip technologies established for a variety of tissues and organs[52,53]. For the inclusion of biomechanical stimulation some of these microfluidic systems used pneumatic actuation for a heart-on-a-chip system[73] or the inclusion of elastomeric membranes for lungs-on-a-chip[74] and for pulmonary artery smooth muscle cells (PASMCs)[57] for example. To our knowledge no other biochip for 3D tenocyte cultivation including biomechanical strain was published so far, but there are some 3D approaches for the culture of tenocytes. Barsby *et al.* (2014) used silicone coated six-well-plates and 0.2 mm minutien pins for the differentiation of embryonic stem cells to tendon tissue. The pins in this set-up were placed 15 mm apart[11], which is almost twice the distance used in our chip setting. For each construct Barsby *et al.* (2014) used 200 µL of collagen suspension and a final concentration of 400000 cells per mL. For RNA isolation, they used 6 to 9 constructs in total.

A recent example for an *in vitro* model exerting biomechanical strain was published by Kataoka *et al.* (2020) using a mechanical cell stretch device (Shellpa Pro, Menicon Co., Ltd./Life Science Department, Aichi, Japan)[75]. Unlike using primary tenocytes as in our experiments, they used a special line of MSCs and reported that Mkx expression combined with cyclic mechanical stretching leads to generation of tendon/ligament-like tissue[75]. To embed the cells in a 3D culture, Kataoka *et al.* (2020) used collagen as well but additionally introduced a mixture of pro-survival factors to minimize cell-death in long-term culture. A major difference to our system is, that rather than applying strain for a short period of time each day, the cell-stretch device used by Kataoka *et al.* (2020) exerted cyclic biomechanical stretching forces all day, gradually increasing the strain for 7 days: 2% (day 1), 4% (day 2), 5% (day 3), 8% (day 4), and 10% (day 5 to 7). Further, they tried to establish an environment that would induce tendon maturation from progenitor cells rather than mimicking a mature native tendon, as we did. Although we could not determine the influence of the mechanical culture component on the tendon organoid in our experiments, the findings of Kataoka *et al.* (2020) emphasize the importance of biomechanical stimuli for the tendon lineage and a modified cell stretch device as used for their experiments would possibly be applicable for tendons-on-a-chip as well.

To ensure the standardized inclusion of mechanic strain in our biochip design, the future stretching device must be optimized and is required to apply strain in an automatized manner without the need of manual assistance. Therefore, the future system must include engines that are strong enough to power the system over a longer period of time and ultimately allow for simultaneous stimulation of more than one chip. Further, the system should be placed in the incubator to ensure stable environmental conditions. As a result, there would be no more need to unmount the chips from the device or to remove them from the incubator (except for changing the medium) which minimizes processing and the risk of unwanted differences. Additionally, in future experiments different strains and frequencies could be applied to mimic physiologic and pathophysiologic tendon loading, which would also enable to mimic different states of tendinopathy more accurately. Another option to improve the biomechanical stimuli conducted to the organoid, would be further adaptation of the collagen concentrations.

In conclusion, tendons-on-a-chip remain a promising *in vitro* model to study tendon physiology and pathophysiology. The chip design established here represents a first step for successful (long-term) culture of equine tenocytes as a 3D organoid. Based on the findings of this thesis further optimization steps are needed to accurately mimic a natural tendon in an on-the-chip environment including biomechanical stimulation.

5. Summary & Zusammenfassung

5.1 Summary

Tendons transfer muscle forces to bones and therefore play a crucial role in locomotion. They are frequently injured due to the enormous loads they are exposed to. About 25 % of the adult population suffer from tendon injuries (tendinopathy). In athletes, 30-50 % of all sport related injuries affect tendons. An equally high rate is observed in sports-horses. The similar pathophysiology between human and equine tendinopathies makes the horse an ideal model of naturally occurring tendon pathologies. Moreover, the superficial digital flexor tendon (SDFT) of the horse has a comparable size to the human Achilles tendon and is functionally equivalent. Tendon lesions usually lead to enduring pain and limited mobility, as injured tendons form scar tissue, which has impaired biomechanical properties and is prone to reinjury. Treatment options are few, mainly focusing on pain relief. To better understand the pathophysiology of tendinopathy, explore more effective treatment approaches and simultaneously reduce the need for animal experiments, an accurate *in vitro* disease model is required. Microfluidic organ-on-a-chip technology enables the 3D cultivation of many tissues and organs on biochips. The aim of this project was to establish a 3D tendon-on-a-chip model, which can be subjected to biomechanical strains mimicking a natural tendon. Microfluidic chips and collagen type I hydrogels were used for tenocyte cultivation in a tendon-like organoid. The contained tenocytes exert forces which contract the hydrogel to a tendon-like structure. Tendon organoids have been successfully cultured on the biochip for up to 28 days. The chip system was either subjected to dynamic strain and relaxation cycles, for 15 minutes a day using a Lego® construct, or to treatments that should imitate a tendinopathic state. Further optimization steps will be required, however the obtained preliminary results will serve as basis for future tendons-on-a-chip which can be used as a disease model to screen for new drugs and treatment options.

5.2 Zusammenfassung

Sehnen übertragen muskulär generierte Kräfte auf Knochen und spielen eine maßgebliche Rolle in der Bewegung. Durch die enormen Belastungen denen Sehnen ausgesetzt sind, kommt es häufig zu Verletzungen. Etwa 25 % der Erwachsenen leiden an Sehnenverletzungen. Bei Athleten betreffen 30 bis 40 % der Sportverletzungen Sehnen. Ähnlich hohe Verletzungszahlen für Sehnen werden auch in Sportpferden beobachtet. Die Pathophysiologie equiner und humaner Sehnenverletzungen ist sehr ähnlich, weshalb sich das Pferd gut als natürlicher Modellorganismus für Sehnenverletzungen eignet. Weiters bildet die oberflächliche digitale Beugesehne (SDFT) des Pferdes das funktionelle Äquivalent zur humanen Achilles Sehne. Generell führen Verletzungen der Sehne zu anhaltenden Schmerzen und eingeschränkter Beweglichkeit, da Narbengewebe mit verringerter biomechanischer Kapazität gebildet wird. Es gibt nur wenige Behandlungsmethoden, welche hauptsächlich auf Schmerzlinderung abzielen. Um die Pathophysiologie von Sehnenerkrankungen besser verstehen zu können, sowie gleichzeitig neue Therapiemethoden zu erforschen und die Notwendigkeit von Tierversuchen zu reduzieren, braucht es ein adäquates *in vitro* Modell. Die „Organ-on-a-chip“ Technologie ermöglicht die dreidimensionale Kultivierung von verschiedenen Geweben und Organen auf sogenannten „Biochips“. Ziel dieser Arbeit war es ein 3D Sehnen-on-a-chip Modell zu entwickeln, auf welches biomechanischer Zug ausgeübt werden kann. Biochips und Kollagen-Typ-I-Hydrogele wurden genutzt, um equine Tenozyten in einem sehnenartigen Organoid zu kultivieren. Die Tenozyten kontrahieren die kollagene Matrix zu einer sehnenartigen Struktur, welche für bis zu 28 Tage erfolgreich auf dem Biochip weiterkultiviert werden konnte. Das Chip-System wurde weiters entweder täglich für 15 Minuten mittels einem Lego®-Konstrukt mit zyklischem Zug stimuliert, oder wurde künstlich in einen Zustand versetzt, der einer Sehnenerkrankung gleicht. Der Chip muss noch weiter optimiert werden; die vorläufigen Erkenntnisse bilden jedoch eine Basis für weitere Sehen-on-a-chip Modelle, welche als Krankheitsmodell zur Erforschung neuer Behandlungsmöglichkeiten dienen können.

6. References

1. Walden, G. *et al.* A Clinical, Biological, and Biomaterials Perspective into Tendon Injuries and Regeneration. *Tissue Eng. - Part B Rev.* **23**, 44–58 (2017).
2. Yan, Z., Yin, H., Nerlich, M., Pfeifer, C. G. & Docheva, D. Boosting tendon repair: interplay of cells, growth factors and scaffold-free and gel-based carriers. *J. Exp. Orthop.* **5**, 1–13 (2018).
3. Thorpe, C. T., Udeze, C. P., Birch, H. L., Clegg, P. D. & Screen, H. R. C. Capacity for sliding between tendon fascicles decreases with ageing in injury prone equine tendons: A possible mechanism for age-related tendinopathy? *Eur. Cells Mater.* **25**, 48–60 (2012).
4. Yang, Z. *et al.* Effect of tendon stem cells in chitosan/β- glycerophosphate/collagen hydrogel on achilles tendon healing in a rat model. *Med. Sci. Monit.* **23**, 4633–4643 (2017).
5. Kannus, P. Structure of the tendon connective tissue. *Scand. J. Med. Sci. Sport.* **10**, 312–320 (2000).
6. Jorgensen, J. S., Genovese, R. L., Ross, M. W. & Dyson, S. J. Superficial Digital Flexor Tendonitis. in *Diagnosis and Management of lameness in the horse* (eds. Ross, M. W. & Dyson, S. J.) 628–672 (Saunders, 2003).
7. Patterson-Kane, J. C., Becker, D. L. & Rich, T. The Pathogenesis of Tendon Microdamage in Athletes: The Horse as a Natural Model for Basic Cellular Research. *J. Comp. Pathol.* **147**, 227–247 (2012).
8. Avella, C. S. & Smith, R. K. W. Diagnosis and Management of Tendon and Ligament Disorders. in *Equine Surgery* (eds. Auer, J. A. & Stick, J. A.) 1157–1179 (Saunders, 2012).
9. Scott, A., Backman, L. J. & Speed, C. Tendinopathy: Update on pathophysiology. *J. Orthop. Sports Phys. Ther.* **45**, 833–841 (2015).
10. Theodossiou, S. K. & Schiele, N. R. Models of tendon development and injury. *BMC Biomed. Eng.* **1**, 1–41 (2019).

11. Barsby, T., Bavin, E. P. & Guest, D. J. Three-dimensional culture and transforming growth factor beta3 synergistically promote tenogenic differentiation of equine embryo-derived stem cells. *Tissue Eng. - Part A* **20**, 2604–2613 (2014).

12. Kolar, R. Animal Experimentation. *Sci. Eng. Ethics* **12**, 111–122 (2006).

13. Huh, D., Hamilton, G. A. & Ingber, D. E. From Three-Dimensional Cell Culture to Organs-on-Chips. *Trends Cell Biol* **21**, 745–754 (2011).

14. Kimura, H., Sakai, Y. & Fujii, T. Organ/body-on-a-chip based on microfluidic technology for drug discovery. *Drug Metab. Pharmacokinet.* **33**, 43–48 (2018).

15. Santoso, J. W. & Mccain, M. L. Neuromuscular disease modeling on a chip. *Co. Biol. Ltd* **2**, (2020).

16. Van Den Berg, A., Mummery, C. L., Passier, R. & Van der Meer, A. D. Personalised organs-on-chips: functional testing for precision medicine. *Lab Chip* **19**, 198–205 (2019).

17. Ergir, E., Bachmann, B., Redl, H., Forte, G. & Ertl, P. Small force, big impact: Next generation organ-on-a-chip systems incorporating biomechanical cues. *Front. Physiol.* **9**, 1–8 (2018).

18. Doblaré, M. & Merodio, J. An Introduction to Biomechanics. in *Biomechanics* (ed. Catterall, R. C. F.) 1–37 (UNESCO-EOLSS, 2015). doi:10.1302/0301-620x.50b1.242.

19. Frank, C. B. & Hart, D. A. The Biology of Tendons and Ligaments. in *Biomechanics of Diarthrodial Joints* (eds. Ratcliffe, A., Woo, S. L. & Mow, V. C.) 39–62 (Springer, 1990).

20. Smith, R. K. W. Pathophysiology of Tendon Injury. in *Diagnosis and Management of lameness in the horse* (eds. Ross, M. W. & Dyson, S. J.) 616–628 (Saunders, 2003).

21. Docheva, D. *et al.* Biologics of Tendon Repair. *Adv. Drug Deliv. Rev.* **84**, 222–239 (2015).

22. Bordoni, B. & Varacallo, M. Anatomy, Tendons. *StatPearls* https://www.ncbi.nlm.nih.gov/books/NBK513237/ (2020).

23. Bi, Y. *et al.* Identification of tendon stem / progenitor cells and the role of the extracellular matrix in their niche. *Nat. Med.* **13**, 1219–1227 (2007).

24. Gaut, L. & Duprez, D. Tendon development and diseases. *Wiley Interdiscip. Rev. Dev. Biol.* **5**, 5–23 (2016).

25. Moshiri, A., Oryan, A., Meimandiparizi, A. & Maffulli, N. Collagen implants in experimental tendon injury in rabbits: A clinical, ultra-structural and biomechanical investigation. *J. Biol. Regul. Homeost. Agents* **28**, 381–397 (2014).

26. Wezenbeek, E. *et al.* What does normal tendon structure look like? New insights into tissue characterization in the Achilles tendon. *Scand. J. Med. Sci. Sport.* **27**, 746–753 (2017).

27. Aicale, R., Tarantino, D. & Maffulli, N. Basic Science of Tendon. in *Use of Stem Cells in Orthopaedics* (eds. Alberto, G., João, E.-M., Lane, J. G. & Karahan, M.) 249–273 (Springer, 2017).

28. Steinmann, S., Pfeifer, C. G., Brochhausen, C. & Docheva, D. Spectrum of tendon pathologies: Triggers, trails and end-state. *Int. J. Mol. Sci.* **21**, (2020).

29. Morita, W., Dakin, S. G., Snelling, S. J. B. & Carr, A. J. Cytokines in tendon disease: A systematic review. *Bone Jt. Res.* **6**, 656–664 (2017).

30. Cook, J. L., Feller, J. A., Bonar, S. F. & Khan, K. M. Abnormal tenocyte morphology is more prevalent than collagen disruption in asymptomatic athletes' patellar tendons. *J. Orthop. Res.* **22**, 334–338 (2004).

31. Bonilla-Gutiérrez, A. F., López, C. & Carmona, J. U. Regenerative Therapies for the Treatment of Tenodesmic Injuries in Horses. *J. Equine Vet. Sci.* **73**, 139–147 (2019).

32. Riley, G. Tendinopathy - From basic science to treatment. *Nat. Clin. Pract. Rheumatol.* **4**, 82–89 (2008).

33. Caliari, Steven R.; Burdick, J. A. A Practical Guide to Hydrogels for Cell Culture. *Nat Methods* **13**, 405–414 (2016).

34. Kuntz, L. A. *et al.* Biomarkers for tissue engineering of the tendon-bone interface. *PLoS One* **13**, 1–24 (2018).

35. Chimenti, R. L., Cychosz, C. C., Hall, M. M. & Phisitkul, P. Current Concepts Review Update: Insertional Achilles Tendinopathy. *Foot Ankle Int.* **38**, 1160–1169 (2017).

36. Dean, B. J. F. *et al.* The risks and benefits of glucocorticoid treatment for tendinopathy: A systematic review of the effects of local glucocorticoid on tendon. *Semin. Arthritis Rheum.* **43**, 570–576 (2014).

37. Lopes, M. A. F., Sullins, K. E. & Walker, B. L. Tenoscopy in 33 horses with septic and nonseptic digital tenosynovitis (1997-2001). *J. Equine Vet. Sci.* **26**, 27–31 (2006).

38. Wang, J. H. C. Can PRP effectively treat injured tendons? *Muscles. Ligaments Tendons J.* **4**, 35–37 (2014).

39. Wang, A. *et al.* Autologous tenocyte injection for the treatment of severe, chronic resistant lateral epicondylitis: A pilot study. *Am. J. Sports Med.* **41**, 2925–2932 (2013).

40. Schwab, L. M., Blanch, P. & Young, M. Autologous tenocyte implantation into shoulder tendon pathology in an elite swimmer. *Phys. Ther. Sport* **29**, 19–25 (2018).

41. Oyeleye, O. O., Ogundeji, S. T., Ola, S. I. & Omitogun, O. G. Basics of animal cell culture: Foundation for modern science. *Biotechnol. Mol. Biol. Rev.* **11**, 6–16 (2016).

42. Schmitz, S. *Der Experimentator: Zellkultur*. *Der Experimentator: Zellkultur* (2011). doi:10.1007/978-3-8274-2573-7.

43. Lerman, M. J., Lembong, J., Gillen, G. & Fisher, J. P. 3D printing in cell culture systems and medical applications. *Appl. Phys. Rev.* **5**, (2018).

44. Yuan, H., Xing, K. & Hsu, H. Y. Trinity of three-dimensional (3D) scaffold, vibration, and 3D printing on cell culture application: A systematic review and indicating future direction. *Bioengineering* **5**, (2018).

45. Haycock, J. W. Chapter 1 and Techniques. in *3D Cell Culture: Methods and Protocols, Methods in Molecular Biology* vol. 695 1–15 (2011).

46. Lee, J., Cuddihy, M. J. & Kotov, N. A. Three-dimensional cell culture matrices: State of the art. *Tissue Eng. - Part B Rev.* **14**, 61–86 (2008).

47. Jensen, C. & Teng, Y. Is It Time to Start Transitioning From 2D to 3D Cell Culture? *Front. Mol. Biosci.* **7**, 1–15 (2020).

48. Pampaloni, F., Reynaud, E. G. & Stelzer, E. H. K. The third dimension bridges the gap between cell culture and live tissue. *Nat. Rev. Mol. Cell Biol.* **8**, 839–845 (2007).

49. Lv, Q., Hu, K., Feng, Q. L. & Cui, F. Fibroin/collagen hybrid hydrogels with crosslinking method: Preparation, properties, and cytocompatibility. *J. Biomed. Mater. Res. - Part A* **84**, 198–207 (2008).

50. Bhatia, S. N. & Ingber, D. E. Microfluidic organs-on-chips. *Nat. Biotechnol.* **32**, 760–772 (2014).

51. Sosa-Hernández, J. E. *et al.* Organs-on-a-chip module: A review from the development and applications perspective. *Micromachines* **9**, (2018).

52. Wu, Q. *et al.* Organ-on-a-chip: Recent breakthroughs and future prospects. *Biomed. Eng. Online* **19**, 1–19 (2020).

53. Jodat, Y. A. *et al.* Human-Derived Organ-on-a-Chip for Personalized Drug Development. *Curr. Pharm. Des.* **24**, 5471–5486 (2018).

54. Takebe, T., Zhang, B. & Radisic, M. Synergistic Engineering: Organoids Meet Organs-on-a-Chip. *Cell Stem Cell* **21**, 297–300 (2017).

55. Mittal, R. *et al.* Organ-on-chip models: Implications in drug discovery and clinical applications. *J. Cell. Physiol.* **234**, 8352–8380 (2019).

56. Kim, W., Kim, J., Park, H. S. & Jeon, J. S. Development of microfluidic stretch system for studying recovery of damaged skeletal muscle cells. *Micromachines* **9**, 1–12 (2018).

57. Sato, K., Nitta, M. & Ogawa, A. A microfluidic cell stretch device to investigate the effects of stretching stress on artery smooth muscle cell proliferation in pulmonary arterial hypertension. *Inventions* **4**, 1–11 (2019).

58. Mustikka, M. P., Pietilä, E. M., Mykkänen, A. K. & Grönthal, T. S. C. Comparison of two rebound tonometers in healthy horses. *Vet. Ophthalmol.* **23**, 892–898 (2020).

59. Schindelin, J. *et al.* Fiji - an Open platform for biological image analysis. *Nat. Methods* **9**, (2009).

60. Dowling, B. A. & Dart, A. J. Mechanical and functional properties of the equine superficial digital flexor tendon. *Vet. J.* **170**, 184–192 (2005).

61. Moro, F. L. *et al.* Horse-like walking, trotting, and galloping derived from kinematic Motion Primitives (kMPs) and their application to walk/trot transitions in a compliant quadruped robot. *Biol. Cybern.* **107**, 309–320 (2013).

62. Ren, K., Zhou, J. & Wu, H. Materials for microfluidic chip fabrication. *Acc. Chem. Res.* **46**, 2396–2406 (2013).

63. Tkachenko, E., Gutierrez, E., Ginberg, M. H. & Groisman, A. An easy to assemble microfluidic perfusion device with a magnetic clamp. *Lab Chip* **9**, 1085–1095 (2009).

64. Weisel, J. W. & Litvinov, R. I. Mechanisms of fibrin polymerization and clinical implications. *Blood* **121**, 1712–1719 (2013).

65. Valero, C., Amaveda, H., Mora, M. & García-Aznar, J. M. Combined experimental and computational characterization of crosslinked collagen-based hydrogels. *PLoS One* **13**, 1–16 (2018).

66. Liang, Y. *et al.* A cell-instructive hydrogel to regulate malignancy of 3D tumor spheroids with matrix rigidity. *Biomaterials* **32**, 9308–9315 (2011).

67. Engler, A. *et al.* Substrate Compliance Vs Ligand Density. *Biophys. J.* **86**, 1–12 (2003).

68. Wilkie, D. A. & Gilger, B. C. Equine glaucoma. *Vet. Clin. North Am. - Equine Pract.* **20**, 381–391 (2004).

69. Yamato, M., Adachi, E., Yamamoto, K. & Hayashi, T. Condensation of collagen fibrils to the direct vicinity of fibroblasts as a cause of gel contraction. *J. Biochem.* **117**, 940–946 (1995).

70. Nomura, M. *et al.* Active expression of matrix metalloproteinase-13 mRNA in the granulation tissue of equine superficial digital flexor tendinitis. *J. Vet. Med. Sci.* **69**, 637–639 (2007).

71. Wang, L. & Stegemann, J. P. Extraction of High Quality RNA from Polysaccharide Matrices using Cetlytrimethylammonium Bromide. *Biomaterials* **31**, 1–14 (2010).

72. Legerlotz, K., Jones, E. R., Screen, H. R. C. & Riley, G. P. Increased expression of IL-6 family members in tendon pathology. *Rheumatol. (United Kingdom)* **51**, 1161–1165 (2012).

73. Marsano, A. *et al.* Beating heart on a chip: A novel microfluidic platform to generate functional 3D cardiac microtissues. *Lab Chip* **16**, 599–610 (2016).

74. Huh, D. A human breathing lung-on-a-chip. *Ann. Am. Thorac. Soc.* **12**, S42–S44 (2015).

75. Kataoka, K. *et al.* In vitro Neo-Genesis of Tendon/Ligament-Like Tissue by Combination of Mohawk and a Three-Dimensional Cyclic Mechanical Stretch Culture System. *Front. Cell Dev. Biol.* **8**, 1–14 (2020).

7. Appendix

7.1 Index of Tables and Figures

7.1.1 Tables

7.1.2 Figures

7.2 Abbreviations

ACTA2 ..... *actin alpha 2, aortic smooth muscle*

AdMSCS ..... *adipose tissue mesenchymal stem cells*

AKAP12 ..... *A-kinase anchor protein 12*

APOA1 ..... *apolipoprotein A*

AT ..... *Achilles tendon*

ATI ..... *autologous tenocyte injection*

BMA ..... *bone marrow aspirate*

BM-MSCs ..... *bone marrow mesenchymal stem cells*

CAD ..... *computer-aided design*

CA3 ..... *Caronic anhydrase 3*

CDET ..... *common digital extensor tendon*

cDNA ..... *complementary DNA*

CNN2 ..... *Calponin-2*

CNRIP1 ..... *CB1 cannabinoid receptor-interacting protein 1*

Col1a1 ..... *collagen type I alpha 1*

Col1a2 ..... *collagen type I alpha 2*

COMP ..... *cartilage oligomeric protein*

CTAB ..... *cetyltrimethylammonium bromide*

DCN ..... *decorin*

DDFT ..... *deep digital flexor tendon*

DEPC ..... *diethylpyrocarbonate*

DMEM ..... *Dulbecco's Modified Eagle Medium*

DMSO ..... *dimethyl sulfoxide*

DNA ..... *deoxyribonucleic acid*

ECM ..... *extracellular matrix*

Egr1 ..... *early growth response 1*

Egr2 ..... *early growth response 2*

ESWT ..... *extracorporeal shock wave therapy*

EtOH ..... *ethanol*

FABP5 ..... *fatty-acid binding protein 5*

FCS ..... *fetal calf serum*

FDA ..... *fluorescin diacetate*

GAPDH *glycerinaldehyd-3-phosphat-dehydrogenase*

IL-1β ..... *interleukin 1 β*

IL-6 ..... *interleukin 6*

IL-10 ..... *interleukin 1*

KERA ..... *Keratokan*

Mkx ..... *Mohawk*

MMP ..... *matrix metalloproteinase*

MMP13 ..... *matrix metalloproteinase 13*

MRI ..... *magnetic resonance imaging*

MSCs ..... *mesenchymal stem cells*

MTT ..... *3-(4,5-Dimethylthiazol-2-yl)-2,5-diphenyltetrazoliumbromid*

MYOC ..... *Myocilin*

NSAIDs ..... *non-steroidal anti-inflammatory drugs*

OOAC ..... *organ-on-a-chip*

OTOR ..... *Otoraplin*

PASMCs ..... *pulmonary artery smooth muscle cells*

PBS ..... *phosphate buffered saline*

PDMS ..... *polydimethylsiloxane*

PES ..... *phenazine ethosulfate*

PGE2 ..... *prostaglandin E2*

PI ..... *propidium iodide*

PLIN4 ..... *Perilipin-4*

PPIA ..... *peptidylprolyl isomerase A*

PRP ..... *platelet rich plasma*

qPCR ..... *quantitative PCR*

rDNase ..... *recombinant DNase*

RNA ..... *ribonucleic acid*

rRNA ..... *ribosomal RNA*

tRNA ..... *transfer RNA*

RPLP0 / 36B4 ..... *acidic ribosomal phosphoprotein P0*

Scx ..... *Scleraxis*

SDFT ..... *superficial digital flexor tendon*

TGF-β ..... tumor growth factor beta

THBS4 ..... *thrombospondin-4*

TNC ..... *tenascin – C*

TNF-α ..... tumor necrosis factor alpha

TNMD ..... *tenomodulin*

TSCs ..... *tendon stem cells*

TSPCs ..... *tendon stem/progenitor cells*

UV ..... *ultraviolet*

2D ..... *two-dimensional*

3D ..... *three-dimensional*

18S ..... *18S ribosomal RNA*